

**[BMIM][BF₄] Incorporation into ZIF-8: Gas Storage and Separation
Performance**

by

Burak Koyutürk

**A Thesis Submitted to the
Graduate School of Engineering
in Partial Fulfillment of the Requirements**

for the Degree of

Master of Science

In

Chemical and Biological Engineering

Koç University

July 2017

Koc University

Graduate School of Sciences and Engineering

This is to certify that I have examined this copy of a master's thesis by

Burak Koyutürk

and have found that it is complete and satisfactory in all respects,
and that any and all revisions required by the final
examining committee have been made.

Committee Members:

Assoc. Prof. Seda Keskin Avcı (Advisor, Koç University)

Asst. Prof. Alper Uzun (Advisor, Koç University)

Assoc. Prof. Uğur Ünal (Koç University)

Prof. Levent Demirel (Koç University)

Prof. Ramazan Yıldırım (Boğaziçi University)

Date:

ABSTRACT

Gas storage and separation processes have been playing a significant role to overcome energy shortage. Both CH₄ and CO₂ exist in the natural gas; CH₄ is considered as a clean energy source, while CO₂ is an impurity which causes to corrosion in the pipelines and decreases the energy content of the natural gas. In the storage and separation processes of these gases, Metal organic frameworks (MOFs) are nominated as promising materials due to their high surface area and large porosities. Modification of MOFs to reach higher gas storage capacities and better separation performances has been recently started.

In the first part of this thesis, incorporation of ionic liquids (ILs) into the pores of MOFs with different loadings (wt%) was investigated. [BMIM][BF₄]/ZIF-8 samples were characterized using different techniques including X-Ray Diffraction (XRD), Thermogravimetric Analysis (TGA), Brunauer–Emmett–Teller (BET) Surface Area, Fourier Transform Infrared (FT-IR) and Scanning electron microscope (SEM). Gas uptakes of the samples prepared were measured using volumetric analysis and gas separation performances were found calculating ideal selectivities. For each sample, different gas storage and separation performances were obtained as a result of the distinct IL-MOF interactions. Results showed that 30 wt% IL-loaded MOF samples are promising materials for especially CO₂/CH₄ and CO₂/N₂ separation applications where the corresponding selectivities increased from 2.2 to 4 and 6.5 to 13.3 at 0.1 bar, respectively. 20 wt% loading can be used for storage purposes as CO₂ uptake increased by 9% at 0.1 bar.

In the second part of this thesis, we extended the IL-MOF pairs and studied several combinations. Same characterization techniques were used for different IL incorporations into ZIF-8 and the relationship between IL-MOF interactions and performances of composite materials was examined. ZIF-8 was modified with annealing process to investigate the CH₄, CO₂ and N₂ static adsorption capacities and separation performances.

IL incorporation into MOF offers opportunity for improvement in gas storage and separation applications. Results showed that these composite materials can be used in purification of natural gas and flue gas to overcome energy shortage.

ÖZET

Gaz depolama ve gaz ayrımı, enerji probleminin üstesinden gelebilme konusunda önemli bir rol oynamaktadır. CH_4 ve CO_2 doğalgazda bulunmakta ve CH_4 diğer fosil yakıtlara oranla daha temiz bir enerji kaynağı olarak kabul edilirken, CO_2 ise boru hatlarına zarar veren ve doğalgazın enerji içeriğini azaltan bir gaz olarak bilinmektedir. Metal organik yapılar (MOF), bu gazların depolanmasında ve birbirinden ve diğer gaz karışımlarından ayrımında kullanılan önemli malzemelerdir. MOF'lar bu konuda gelecek vadeden malzemeler olduğundan, daha iyi depolama kapasitesine ve daha iyi ayırma performansına ulaşmak için MOF'ların yapıları ve modifikasyonu ile ilgili çalışmalar sürmektedir.

Bu tez çalışmasının ilk bölümünde, iyonik sıvıların farklı yüklemelerde MOF'ların gözeneklerine yerleştirilmesi incelenmiştir. Hazırlanan [BMIM][BF₄]/ZIF-8 örnekleri XRD, BET, FT-IR ve SEM gibi farklı deneysel teknikler kullanılarak karakterize edilmiştir. Gaz depolama performansları volumetrik analiz kullanılarak ölçülmüş ve ideal seçicilikleri hesaplanarak gaz ayırma performansları bulunmuştur. Her bir örnekte İyonik Sıvı ve MOF arasındaki etkileşimden dolayı saf MOF'a göre farklı depolama kapasiteleri olduğu gözlenmiştir. Elde edilen sonuçlar kütlece %30 yüklemeli hibrit malzemelerin, 0,1 bar'da CO_2/CH_4 ve CO_2/N_2 seçiciliklerinin sırasıyla 2,2'den 4'e ve 6,5'tan 13,3'e yükselmesinden dolayı bu gaz ayrımlarında gelecek vadeden malzemeler olduğunu göstermektedir. Kütlece %20 yüklemeli hibrit malzemenin ise CO_2 tutma kapasitesinin 0,1 bar'da %9 artışı, bu malzemenin depolama uygulamaları için uygun olduğunu göstermektedir.

İkinci bölümde, ilk bölümde elde edilen bilgiler ışığında hibrit malzemelerin farklı kombinasyonları incelenmiştir. Aynı karakterizasyon teknikleri kullanılmış ve iyonik sıvı-MOF arasındaki etkileşimler ile gaz tutma ve ayırma performansları arasındaki ilişki araştırılmıştır. Bunun yanı sıra, ZIF-8 tavlama işlemi ile modifiye edilmiş ve CH_4 , CO_2 ve N_2 gazlarının statik tutma kapasiteleri ile gaz ayırma performansları üzerindeki etkisi araştırılmıştır.

MOF'ların gözeneklerine iyonik sıvı hapsedilmesi gaz tutma ve ayırma işlemlerinde iyileştirme sağlamaktadır. Sonuçlar bu malzemelerin doğalgaz ve baca gazı arıtmasında kullanılabileceğini ve enerji problemi için çözüm olabileceğini göstermiştir.

ACKNOWLEDGEMENTS

First of all, I would like to thank my advisors Dr. Alper Uzun and Dr. Seda Keskin for their exceptional support and supervision. They contributed to my vision in academia and my life. I would also like to thank my thesis committee members Dr. Ramazan Yıldırım, Dr. Levent Demirel and Dr. Uğur Ünal for their valuable times and contributions.

I would like to thank my family for their sympathy and support during my master study and standing by me in my every decision.

Nanomaterials, Energy and Molecular Modeling Research Group (NEMO) became my home during this master study. I would like to thank Çiğdem for turning this office into a home for each member. I really appreciate the time Pelin spent with me since the beginning of our master study and her endless patience. I would like to thank İlknur for every contribution she made in my life and to this group. I would also like to thank Zeynep, Elda, Vahid, Ayda, Özge, Derya and Zeeshan for their generous friendship. I feel very lucky to meet the honorary members of NEMO, Benay and Onur. I am very grateful for their wholehearted friendships.

I would like to thank all Uzun Lab members for their helps. I am thankful for especially Ahsan, Melike and Özge's limitless support and friendships.

I am very thankful to Barış Yağcı, Ceren Yılmaz Akkaya and Gülsu Şimşek for their helps in the experiments carried out in Koç University Surface Science and Technology Center (KUYTAM).

This project is funded by Tübitak 1001 Program (project number: 114R093). I sincerely acknowledge the support from Koç University Seed Program, and Koç University-Tüpraş Energy Center (KÜTEM).

TABLE OF CONTENTS

ABSTRACT.....	iii
ÖZET	iv
ACKNOWLEDGEMENTS	v
LIST OF TABLES	viii
LIST OF FIGURES	ix
NOMENCLATURE	xi
Chapter 1: Introduction	1
Chapter 2: Literature Review	4
2.1 IL-Incorporated MOF Composites in Gas Storage and Separation Applications	4
2.1.1 Adsorption-based Gas Separation	4
2.2 Other Applications of Ionic Liquid-Incorporated MOFs	6
Chapter 3: Methods.....	10
3.1 Materials and Sample Preparation.....	10
3.2 Characterization Methods	11
3.2.1 X-Ray Diffraction.....	11
3.2.2 Thermal Gravimetric Analysis	11
3.2.3 Scanning Electron Microscopy	11
3.2.4 Brunauer–Emmett–Teller (BET) Surface Area	12
3.2.5 Infrared Spectroscopy	12
3.2.6 Elemental Analysis.....	13
3.3 High Pressure Volumetric Adsorption Analysis	13
Chapter 4: Preparation, Characterization, and Adsorption Measurements Of [BMIM][BF ₄]/ZIF-8 Samples.....	15
4.1 Preparation of [BMIM][BF ₄]/ZIF-8 Samples	15
4.2 Characterization of ZIF-8, [BMIM][BF ₄] and [BMIM][BF ₄]/ZIF-8 Samples.....	15
4.2.1 Elemental Analysis.....	15
4.2.2 Scanning Electron Microscopy (SEM)	16

4.2.3 Powder X-Ray Diffraction (PXRD).....	18
4.2.4 Brunauer–Emmett–Teller (BET) Surface Area	19
4.2.5 Thermal Gravimetric Analysis (TGA)	20
4.2.6 Infrared (IR) Spectroscopy.....	22
4.3 Performance Measurements	26
4.3.1 Gas Adsorption Analysis of ZIF-8.....	26
4.3.2 Selectivity Calculation and Comparison.....	30
4.4 Heat of Adsorption Measurements.....	34
Chapter 5: Different IL-MOF Pairs	38
5.1 Other IL-MOF Combinations	38
Chapter 6: Annealing of ZIF-8	49
Chapter 7: Conclusions and Outlook	54
Bibliography	56
Appendix A: Supplementary Information for Fit Parameters.....	60
Appendix B: Surface Area/Pore Volume-Loading Correlations	62
Appendix C: Supplementary Information for IR Deconvolution	63
Appendix D: Gas Uptakes and Selectivities	65
Appendix E: Names of Ionic Liquids	69

LIST OF TABLES

Table 4.1: Boron and zinc amounts in IL-incorporated ZIF-8 samples determined by ICP-MS.	16
Table 4. 2: Measured BET surface areas and pore volumes of ZIF-8 and [BMIM][BF ₄]/ZIF-8.	20
Table 4.3: Derivative decomposition temperature ($T'_{\text{onset}}^{[76]}$) of bulk [BMIM][BF ₄], pristine ZIF-8, and [BMIM][BF ₄]/ZIF-8 samples.	22
Table 4. 4: Shifts in IR bands of [BMIM][BF ₄] in the lower region.	25
Table 4. 5: Shifts in IR bands of [BMIM][BF ₄] in the higher region.	25
Table 4.6: Comparison of normalized selectivities of [BMIM][BF ₄]/ZIF-8 with the normalized selectivities of other IL/MOF samples studied in our previous works. ^[32-33] IL loading in MOFs are 30, 26 and 28 wt% for [BMIM][BF ₄]/Cu-BTC, [BMIM][PF ₆]/ZIF-8, and [BMIM][BF ₄]/ZIF-8, respectively.	34
Table 5.1: ILs incorporated into ZIF-8.	39
Table 5.2: XRF results of IL/MOF composites	40
Table 5.3: $\nu(\text{C2H})_{\text{sym}}$ vibration bands of pure ILs and IL/MOF composites.	44
Table A.1: Fit parameters for CO ₂ , CH ₄ and N ₂ measured at different temperatures for ZIF-8.	60
Table A.2: Parameters of dual site Langmuir and Freundlich fits.	60
Table A.3: Fit parameters for IL/MOF composites	61
Table A.4: Fit parameters for Annealed ZIF-8 and [BMIM][PF ₆]/Annealed ZIF-8	61
Table E.1: Full names of ionic liquids mentioned in this thesis.	69

LIST OF FIGURES

Figure 4.1: SEM images of ZIF-8 and [BMIM][BF ₄]/ZIF-8 samples at 100 K \times magnification: (a) ZIF-8, (b) IL ₄ /ZIF-8, (c) IL ₂₀ /ZIF-8, and (d) IL ₂₈ /ZIF-8.....	17
Figure 4.2: EDX results on IL ₂₈ /ZIF-8.	17
Figure 4.3: XRD patterns of ZIF-8 (black) and [BMIM][BF ₄]/ZIF-8 samples: IL ₄ /ZIF-8 (red), IL ₂₀ /ZIF-8 (blue), and IL ₂₈ /ZIF-8 (green).....	18
Figure 4.4: N ₂ isotherms of ZIF-8 and [BMIM][BF ₄]/ZIF-8 samples at 77 K.....	19
Figure 4.5: Thermal stability of pristine ZIF-8, bulk [BMIM][BF ₄], and IL-incorporated samples.....	21
Figure 4.6: Derivative weight change of ZIF-8 and IL/ZIF-8 samples.	21
Figure 4.7: IR spectra of IL-incorporated MOFs, bulk [BMIM][BF ₄] and pristine ZIF-8: (a) 900-1600 cm ⁻¹ , (b) 2800-3200 cm ⁻¹	25
Figure 4.8: Gas uptakes of ZIF-8 and IL-incorporated ZIF-8 obtained from experiments and simulations: (a) ZIF-8, (b) IL ₄ /ZIF-8, (c) IL ₂₀ /ZIF-8, (d) IL ₂₈ /ZIF-8. Filled symbols: experimental uptake values, empty symbols: simulated uptake values multiplied with the factors.....	28
Figure 4.9: Uptake change (%) of CO ₂ , CH ₄ , and N ₂ with respect to IL loading (wt%): (a) 0.1 bar, (b) 0.2 bar, (c) 1 bar, (d) 5 bar. Dotted lines are provided to guide the eye.	30
Figure 4.10: Normalized selectivities of samples (the ratio of IL/ZIF-8 samples to the selectivity of pure ZIF-8) for (a) CO ₂ /CH ₄ , (b) CO ₂ /N ₂ , (c) CH ₄ /N ₂ separations.	33
Figure 4.11: Isothermic heat of adsorption of: (a) ZIF-8, (b) IL ₄ /ZIF-8, (c) IL ₂₀ /ZIF-8, and (d) IL ₂₈ /ZIF-8 calculated by Equation 3.6 using the adsorption isotherms obtained at 10 and 25 °C.	36
Figure 4.12: Change in the isothermic heat of adsorption of corresponding gases in ZIF-8 and IL ₂₈ /ZIF-8 with respect to the gas selectivities. Closed (open) symbols show selectivity of ZIF-8 (IL ₂₈ /ZIF-8) sample. Each symbol indicates different pressure: rectangle (■): 0.1 bar, triangle (▲): 1 bar, circle (●): 5 bar.	37
Figure 5.1: SEM images of IL/MOF composites: (a) [EMIM][PF ₆]/ZIF-8, (b) [OMIM][PF ₆]/ZIF-8, (c) [C ₃ CNMIM][NTf ₂]/ZIF-8, (d) [(EtO) ₂ IM][NTf ₂]/ZIF-8, (e) [EMIM][SCN]/ZIF-8, (f) [BMIM][OcSO ₄]/ZIF-8.....	41

Figure 5.2: XRD pattern of ZIF-8 and IL/MOF Composites.	42
Figure 5.3: IR spectra of ZIF-8, ILs and IL/MOF composites.	44
Figure 5.4: Uptake values in ZIF-8 and IL-MOF composites: (a) CH ₄ , (b) CO ₂ , (c) N ₂	46
Figure 5.5: Selectivities of ZIF-8 and IL-MOF composites: (a) CO ₂ /CH ₄ (b) CO ₂ /N ₂ (c) CH ₄ /N ₂	48
Figure 5.6: Adsorption isotherms of ZIF-8, An-ZIF-8, [BMIM][PF ₆]/ZIF-8, and [BMIM][PF ₆]/An-ZIF-8: (a) CO ₂ , (b) CH ₄ , (c) N ₂	51
Figure 5.7: Selectivity of ZIF-8, An-ZIF-8, [BMIM][PF ₆]/ZIF-8, and [BMIM][PF ₆]/An-ZIF-8.....	53
Figure B.1: Linear correlations: (a) IL loading-surface area (b) IL loading-pore volume.	62
Figure C.1: Deconvoluted IR peaks between 900-1600 cm ⁻¹ (a) IL ₄ /ZIF-8, (b) IL ₂₀ /ZIF-8, (c) IL ₂₈ /ZIF-8 (d) ZIF-8.....	63
Figure C.2: Deconvoluted IR peaks between 2800-3200 cm ⁻¹ : (a) IL ₄ /ZIF-8, (b) IL ₂₀ /ZIF-8, (c) IL ₂₈ /ZIF-8, (d) ZIF-8.	64
Figure D.1: Gas uptakes of ZIF and IL-incorporated ZIF-8 obtained from experiments and simulations (a) IL ₄ /ZIF-8, (b) IL ₂₀ /ZIF-8, (c) IL ₂₈ /ZIF-8. Filled symbols: experimental uptake values, empty symbols: unmodified computational uptake values, plus circle: computational uptake values scaled with the factor.	66
Figure D.2: Ideal adsorption selectivities of ZIF-8 and [BMIM][BF ₄]/ZIF-8 samples calculated from fitted isotherms.....	68

NOMENCLATURE

MOF: Metal organic framework	BET: Brunauer–Emmett–Teller
IL: Ionic liquid	FTIR: Fourier transform infrared
ZIF: Zeolitic imidazolate framework	ATR: Attenuated total reflection
PAHs: Polycyclic aromatic hydrocarbons	ICP-MS: Inductively coupled plasma mass spectrometry
AmPyI: aminopyridinium iodide	XRF: X-Ray Fluorescence
COFs: Covalent organic frameworks	HPVA: High pressure volumetric analyzer
DFT: Density functional theory	Q_{st} : Isosteric heat of adsorption (kJ/mol)
MMMs: Mixed matrix membranes	GCMC: Grand canonical Monte Carlo
Poly(RTIL): Polymerizable room temperature ionic liquid	TGA: Thermal gravimetric analysis
RTILs: room temperature ionic liquids	T_{onset} : Onset temperature (°C)
XRD: X-Ray Diffraction	T'_{onset} : Derivative onset temperature (°C)
PXRD: Powder X-Ray Diffraction	UFF: Universal force field
SEM: Scanning electron microscope	
EDX: Energy dispersive X-Ray spectroscopy	

Chapter 1

INTRODUCTION

Gas storage and separation processes play an important role in the field of energy as the energy demand increased in last few decades as a result of population growth on the Earth. Among the several gases which are used as fuels, CO₂ and CH₄ storage have attracted more interest due to several reasons. CH₄ which is cleaner energy compared to other fossil fuels is the main constituent of natural gas and it has potential to replace petroleum. Lately, utilization of CH₄ in vehicles as fuel has been discussed; however, the challenges in storage of compressed natural gas and liquefied natural gas hinder the increase in demand for natural gas vehicles.^[1]

CO₂ is known as a greenhouse gas which causes the global warming and its concentration is predicted to climb over 450 ppm before 2050.^[2] Apart from its environmental aspect, CO₂ exists in natural gas as impurity and causes corrosion in pipelines.^[3] Therefore, reduction of CO₂ and utilization of captured CO₂ became important lately.^[4]

In order to improve the storage and separation of CO₂ and CH₄, adsorption-based storage and separation have been recently considered. Adsorption is known as enrichment of a solid material or increase in the density of a fluid when exposed to the surface of the material.^[5] Adsorption takes place in many physical, chemical, and biological applications including catalysis, drug delivery, and solid state reactions. Porous materials are used for sorption of gases as adsorbents and their structural properties are significantly related to the storage and separation performances.^[6] There have been many efforts for synthesizing new adsorbent materials and modifying the conventional ones to enhance storage performances. Metal organic frameworks (MOFs) are a new group of materials. MOFs are composed of metal ions and organic linkers and combination of these components provides limitless possibilities.^[7]

More significantly, as MOFs are crystalline materials, the position and the order of the atoms can be found easily.^[8] These ordered materials also exhibit high surface area (up to 7000 m²/g) and tunable pore sizes that allow surface functionalization.^[9] MOFs can be rigid or flexible/dynamic which allow the pore sizes to change at certain conditions.^[10]

Synthesis of MOFs can be carried out with the conventional methods, such as solvothermal and nonsolvothermal as well as alternative methods, such as microwave-assisted, electrochemical, mechanochemical and sonochemical that supply the heat required for the reactions in different ways.^[11] MOFs can also be modified during the synthesis and after synthesis to reach desired properties on certain applications. Tuning the functional groups during the synthesis is challenging due to some limitations related to synthesis conditions, however, after the formation of crystalline structure, MOFs can be modified with post-synthetic methods easier due to the absence of the limitations encountered in synthesis.^[12]

One recent approach to modify MOFs after synthesis is ionic liquid (IL) incorporation into the pores of MOF. ILs which were discovered in 1914 by Paul Walden, are non-volatile organic salts composed of anion and cation.^[13] Their melting points are below 100 °C and more importantly, they are tunable similar to MOFs.^[14] The physicochemical properties of the ILs can be determined depending on the cation-anion combination.^[15] ILs are used as liquid supports for storage and separation of especially toxic gases, stationary phase in chromatographic applications and electrolytes in rechargeable cells.^[16-17]

In this thesis, MOFs modified by IL incorporation were characterized using various techniques. IL-MOF interactions were elucidated and ultimately, the consequences of these interactions on gas storage and separation performances were investigated. Loading amount of [BMIM][BF₄] in the pores of ZIF-8 have been examined and the optimum loading was found as 30 wt%. IL/MOF composites showed remarkable performances on CO₂/CH₄, CO₂/N₂ and CH₄/N₂ separations. Since each IL has distinct physicochemical properties, we expanded our approach to several IL/MOF combinations to understand the relation between the structural properties of ILs and sorption properties of the composites. In Chapter 2, literature review of IL/MOF composites is given and in Chapter 3, methods used to characterize and measure sorption properties of IL/MOF composites are covered. In Chapter 4, characterizations and performances of different [BMIM][BF₄] loadings into ZIF-8 were

illustrated. In Chapter 5, incorporation of other imidazolium-based ILs were examined and in Chapter 6, incorporation of ILs after annealing of ZIF-8 was investigated.



Chapter 2

LITERATURE REVIEW

In this part of the thesis, IL/MOF composites used in different fields were reviewed.

2.1 IL-Incorporated MOF Composites in Gas Storage and Separation Applications

2.1.1 Adsorption-based Gas Separation

A recent technology to fine-tune the gas separation performance of a MOF is to utilize ILs. Similar to MOFs, ILs offer high degree of tunability with almost endless possible combinations of anions and cations.^[18] Thus, combining MOFs with ILs offers tremendous potential in the way of tuning the gas separation performance of these materials.

IL-MOF combinations have been considered experimentally in the gas separation field.^[19-25] Da Silva et al.^[26] impregnated [BMIM][PF₆] and [BMIM][NTf₂] into Cu-BTC at different loadings and concluded that 10 wt% [BMIM][PF₆] loading caused to detrimental effect on textural properties of MOF. Dhumal et al.^[27] studied the interactions between Cu-BTC and 1-ethyl-3-methylimidazolium ethyl sulfate ([EMIM][EtSO₄]) by combining experiments with density functional theory (DFT) calculations and examined the changes in both MOF and IL structures as a result of incorporation of IL into the MOF. Ban et al.^[25] incorporated [BMIM][Tf₂N] into ZIF-8 and reported that CO₂ uptake was enhanced especially at low pressure region whereas CH₄ and N₂ decreased. Their results also showed that CO₂/CH₄ and CO₂/N₂ ideal selectivities increased remarkably (from 7.5 to 41 and 19 to 100, respectively).

Several groups worked on IL/MOF composites in gas storage and separation field computationally. For instance, Chen et al.^[28] performed Grand Canonical Monte Carlo

(GCMC) simulations of 1-butyl-3-methylimidazolium hexafluorophosphate ([BMIM][PF₆]) incorporated IRMOF-1 composite and reported a CO₂/N₂ selectivity of 70 at ambient conditions. To understand the effect of different types of ILs on the separation performances of IL-MOF systems, ILs with the same cations but different anions were studied.^[29-30] However, among the researches considering IL-MOF couples, there are limited number of studies focusing on the elucidation of reasons for better gas selectivities obtained by the incorporation of ILs into the pores of MOFs. Xue et al.^[31] investigated the dispersion of 1-butyl-3-methyl-imidazolium thiocyanate ([BMIM][SCN]) in different MOFs and covalent organic frameworks (COFs) and concluded that better dispersion of IL leads to higher gas separation performances. Moreover, [BMIM][BF₄] was incorporated with different loadings into the cages of Cu-BTC and improvements were observed in CH₄/H₂, N₂/H₂, and CH₄/N₂ selectivities as a consequence of the interactions between IL and MOF.^[32] However, gas separation performance of Cu-BTC was negatively affected due to the interactions of ILs with the open metals sites available in Cu-BTC. Therefore, to study the incorporation of ILs in a different MOF that have saturated metal sites and [BMIM][PF₆] was incorporated into the pores of ZIF-8 to investigate the separation performance of resulting composite.^[33] Remarkable improvements in selectivities were found especially for CO₂/CH₄ and CO₂/N₂ separations at low pressures. Interactions between IL and MOF were examined thoroughly using various characterization methods combined with DFT calculations and molecular simulations to elucidate the effect of these interactions on the gas separation performances. Results indicated that IL/MOF interactions play a crucial role in determining the gas separation performance of the composite. For each IL/MOF combination such interactions must be considered individually and their consequences on the gas separation performance should be described in detail for the rational design of novel IL/MOF composites with exceptional performance. In this thesis, in order to find out the optimum IL loading amount in ZIF-8, [BMIM][BF₄] was incorporated at different loadings, the composites were characterized, and the interactions between IL and MOF were elucidated. The loading that shows the best performance was found as 30 wt% and [EMIM][PF₆]/ZIF-8, [OMIM][PF₆]/ZIF-8, [C3CNMIM][NTf₂]/ZIF-8, [(EtO)₂IM][NTf₂]/ZIF-8, [EMIM][SCN]/ZIF-8, [BMIM][OcSO₄]/ZIF-8, and [BMIM][NTf₂]/ZIF-8 samples were prepared with the same procedure, characterized and performance measurements were carried out.

2.2 Other Applications of Ionic Liquid-Incorporated MOFs

MOFs are the crystalline porous materials with high surface area and porosity. They have recently attracted attention and studied in the intersection of chemistry and materials science as they take the advantage of both organic linkers and metal nodes.^[34] Although synthesis of new MOFs is important, modification of existing MOFs provides opportunity to reach desired properties required for a certain application.^[12] IL incorporation into the pores of MOFs is one of the approaches to modify MOF's structure and it has been recently studied in detail in the literature.^[35-36] IL-incorporated MOF composites can be obtained with different methods such as ionothermal synthesis^[37-38] and post-impregnation of ILs including sub-methods such as wet impregnation,^[21-22, 26, 32-33, 39-51] capillary action^[27, 52-56] and ship-in-a bottle^[57-60] methods. IL-incorporated MOF composites were investigated in various applications both experimentally and computationally.

Liquid phase adsorption and separation is one of the fields that IL-incorporated MOFs have been studied. Mostly, removal of toxic compounds, hydrocarbons or ions from the liquids were aimed. Khan et al.^[39] examined the sulfur removal from liquid fuel using acidic IL ([BMIM][Cl]) incorporated in MIL-101(Cr). They found that performance of MOF increased by 71% as a result of acid-base interactions between IL and benzothiophene. They considered different IL loadings and obtained the highest performance with 33 wt% loading. At higher loadings, due to the occupation of pores with IL, diffusion of guest molecules are blocked. They also studied the removal of sulfur using different IL ([BMIM][Br]) with the same MOF and observed enhancement compared to the pure MOF.^[58] Apart from the separation performance, they illustrated that IL-incorporated MOF can be used many times and once they are regenerated, they show the same performance with the fresh ones.

Another study focused on separation of polycyclic aromatic hydrocarbons (PAHs) from water, vegetable and fruit juice with IL/MOF composites.^[47] [BMIM][Cys]/MIL-100(Fe) was used to adsorb PAHs selectively and results suggested that the performance of MIL-100(Fe) was increased by 97-103.5% with incorporation of [BMIM][Cys]. A similar research was conducted by Nasrollahpour and Moradi to examine the removal of chromate ion from water.^[45] They used acidic chloroaluminate IL and MIL-100(Fe) and prepared composite

with wet impregnation method. Results showed that IL-incorporated MOF composite demonstrated higher Cr(VI) capacity than pristine MOF and other novel adsorbents.

MOFs have been studied in the field of catalysis since they show catalytic activity due to their large internal surface areas.^[61] A number of ILs was used to tune the catalytic activity and selectivity of MOFs in the literature.^[21, 44, 62-65] For example, ZIF-90 was functionalized with aminopyridinium iodide (AmPyI) and the resulting materials showed better activity than pure ZIF-90 in cyclic carbonates with the cycloaddition of CO₂.^[63] Another IL/MOF composite was prepared with direct ligand modification and resulting material is referred as bifunctional as it indicates CO₂ selective adsorption and catalyst properties for cycloaddition of CO₂.^[66] When IL/MOF composites was used with co-catalyst TBAB (n-Bu₄NBr) the yield was increased to 99% at 90 °C over 3 hours reaction.

Luo et al. incorporated Brønsted acidic imidazole based BAIL (IMIZ-BAIL) and triethylene diamine based-BAIL (TEDA-BAIL) separately to MIL-101(Cr) to modify catalytic activity. They elucidated the interactions between ILs and MOF, and examined the performances of IL-incorporated MOF composites in the acetalization of benzaldehyde with glycol. Both ILs improved the activity but TEDA-BAIL/MIL-101(Cr) showed better performance due to the higher dispersion of IL. They also incorporated amino-functionalized basic IL (ABIL-OH) into the pores of Cu-BTC and investigated the performance of the composite upon Knoevenagel condensation.^[40] ABIL-OH/CuBTC catalyst showed a size- and shape-selective property and as the highest conversion (100%) was achieved with the smallest size of reactant whereas the lowest conversion (12%) was obtained with the largest size reactant.

Wu et al.^[51] impregnated [PSMIM][HSO₄] in the pores of UiO-66 to examine the utilization of the composite in the oxidative desulfurization (ODS) of fuel oils. [PSMIM][HSO₄]/UiO-66 exhibited better desulfurization performance than pristine UiO-66. Loading of IL also plays an important role in the performance as it increased from 62.3% to 92.9% when loading increases from 10 wt% to 50 wt%. They achieved the removal of 90.6% benzothiophene with the composite.

Chen et al.^[42] used the IL/MOF composites in biodiesel production. They took the advantage of the catalytic activity of Cu-BTC and incorporated Brønsted acidic IL, [HVIm-(CH₂)₃SO₃H]HSO₄, into Cu-BTC. Catalytic performance was measured using the esterification reaction of oleic acid and ethanol. IL incorporation led to an increase to 92.1% from 10% in the conversion.

Abednatanzi et al.^[48] used dual amino-functionalized ionic liquid (DAIL) incorporated MIL-100(Fe) as support for immobilization of polyoxometalate (POM) ($H_3PW_4O_{24}$) in the selective oxidation of benzyl alcohol. Resulting material ($PW_4/DAIL/MIL-100(Fe)$) with 1.2 mmol/g IL loading, demonstrated 92% conversion and selectivity greater than 99% whereas pristine MIL-100(Fe) showed 38% conversion. They also investigated the catalytic performance of different POM ($H_3PW_{12}O_{40}$) and MOF (MIL-101(Cr)) pair with the same IL (DAIL).^[49] They reported that the resulting sample ($HPW/DAIL/MIL-101(Cr)$) overperformed the pristine MOF and IL-free catalyst in terms of conversion and thermal stability.

IL/MOF composites have been studied in membrane based gas separations recently. Mixed matrix membranes (MMMs) contain a bulk polymer and an inorganic particle phase.^[67] MMMs offer opportunity to reach superior gas separation properties and stability. To overcome the Robeson upper bound^[68-69] which is plotted as a result of a selectivity versus permeability tradeoff, MMMs were modified with IL incorporation.

Ban et al.^[25] investigated the confinement of $[BMIM][Tf_2N]$ into ZIF-8 and separation performance of polysulfone (PSF) including IL/MOF nanoparticles. Their data indicated a significant improvement in the selectivity and permeability for CO_2/CH_4 and CO_2/N_2 .^[25] Casado et al.^[19] studied similar MMMs prepared by $[EMIM][Ac]$, chitosan (CS) and ZIF-8 or HKUST-1 which is known as Cu-BTC commercially. They added ZIF-8 and Cu-BTC into IL-CS hybrid membranes at different loadings (5-20 wt%) and reported the CO_2/N_2 selectivity performances of 10 wt% ZIF-8/IL-CS and 5 wt% HKUST-1/IL-CS MMMs as 11.5 and 19.3 at 50 °C and 2 bar. Hao et al.^[20] conducted a research to understand the effects of ZIF-8 in the mixture of polymerizable room temperature ionic liquids (poly(RTIL)) and free room temperature ionic liquids (RTILs). They found that addition of 25.8 wt% ZIF-8 to a miscible ionic liquid blend system increases the permeability but decreases the CO_2/CH_4 and CO_2/N_2 selectivities of $P[vbim][NTf_2]/[emim][B(CN)_4]/ZIF-8$, which was prepared with 1-vinyl-3-butylimidazolium-bis(trifluoromethyl-sulfonyl)imidate ($[vbim][NTf_2]$) and 1-ethyl-3-methylimidazoliumtetracyanoborate ($[emim][B(CN)_4]$) and ZIF-8, from 15.8 to 12.3 and from 29.9 to 24.2, respectively. Li et al.^[33] incorporated $[BMIM][Tf_2N]$ into ZIF-8 and prepared IL@ZIF-8/Pebax membranes. CO_2/CH_4 and CO_2/N_2 selectivities of IL@ZIF-8/Pebax membranes increased by 92% and 74% over pure Pebax membranes. They also reported improved CO_2 permeability by 45%. Ma et al.^[22] fabricated MMM with a task specific IL, $[C_3NH_2bim][Tf_2N]$, and $NH_2-MIL-101(Cr)$ as MOF and PIM-1. They improved CO_2

permeability and CO₂/N₂ selectivity compared to NH₂-MIL-101(Cr) and PIM-1. They found the CO₂ permeability of composite is 23% higher than PIM-1 membrane for 5 wt% IL loading where CO₂/N₂ selectivity was improved by 119% compared to PIM-1 membrane.

In this study, we prepared a composite from a specific IL/MOF combination, [BMIM][BF₄] and ZIF-8, to investigate the effect IL incorporation and the loading amount on the gas adsorption and adsorption based gas separation performance of pristine ZIF-8. Detailed characterization of the IL-incorporated ZIF-8 samples revealed the interactions between the IL and MOF. The consequences of these interactions on the heat of adsorption of gases, gas uptakes, and the consequent effects on the gas separation performance of the ZIF were evaluated. After the determination of the IL loading that leads to highest gas separation performance (30 wt%), different ILs were impregnated to ZIF-8 and characterization and CO₂/CH₄, CO₂/N₂ and CH₄/N₂ separation performances which are essential in natural gas and flue gas purification were calculated.

Chapter 3

METHODS

This chapter covers experimental methods utilized to characterize and measure the performance of the samples.

3.1 Materials and Sample Preparation

[BMIM][BF₄] and ZIF-8 were purchased from Sigma-Aldrich and stored in an argon-filled Labconco glovebox. N₂ (99.998 vol %), CH₄ (99.95 vol %), and CO₂ (99.9 vol %) were purchased from Linde gas company. IL-incorporated MOF samples were prepared by first activating ZIF-8 at 150 °C overnight under vacuum. For 5 wt % IL loading, 0.05 g of [BMIM][BF₄] was dissolved in 30 mL of acetone (Sigma-Aldrich) and kept mixing for 15 min. After mixing, 0.95 g of ZIF-8 was added into acetone–IL solution, and the resulting solution was mixed on a magnetic stirrer at 100 rpm at 30 °C for several hours until acetone was evaporated. When all acetone was evaporated, the remnant was dried overnight at 105 °C. The resulting sample was moved back to the glovebox until use. The same procedure was followed in the preparation of 20 and 30 wt % loaded ZIF-8 samples. For 20 (30) wt % loading, 0.2 (0.3) g of IL and 0.8 (0.7) g of ZIF-8 were used. The resulting IL loadings in each sample were determined as described below. The samples investigated in the second part of the thesis were prepared following the same procedure.

3.2 Characterization Methods

3.2.1 X-Ray Diffraction

X-Ray Diffraction (XRD) is used for qualification and quantification of the structure of crystals by means of X-Ray generated through a source. In this study, we used Powder X-Ray Diffraction (PXRD) to examine if IL incorporation causes any change in the structure. The X-ray diffraction pattern of each sample was obtained by a Bruker D8 Advance X-ray diffractometer with 40 kV of voltage and 40 mA of current. A Cu K α 1 radiation source with a wavelength of 1.5418 Å and a Vantec-1 detector with 1 mm slit size were used. Measurements were carried out in the range of 2Θ values of 5–50 with a step size of 0.02°.

3.2.2 Thermal Gravimetric Analysis

A TA Instruments Q500 model thermogravimetric analyzer was used for thermogravimetric analyses. Nearly 15 mg of each sample was placed on a platinum pan after taring. For ZIF-8 and [BMIM][BF₄]/ZIF-8 samples, a heating rate of 5 °C/min was employed up to 120 °C and followed by an isothermal treatment at that temperature for 8 h. The temperature was then increased up to 700 °C at a ramp rate of 2 °C/min. For the bulk [BMIM][BF₄], an approximately 15 mg sample was measured. A heating rate of 2 °C/min was employed up to 80 °C, and then the sample was kept isothermal for 5 h. After that, the temperature was raised to 700 °C at 2 °C/min. All measurements were performed under N₂ flow. Same procedure was followed for other ILs and IL/MOF composites.

3.2.3 Scanning Electron Microscopy

Scanning electron microscopes are used for imaging by the interaction between sample and electron beams sent to the surface. SEM images were used to investigate any changes in morphology of MOF upon IL incorporation. Images were obtained by a Zeiss Ultra Plus field emission scanning electron microscope under ultrahigh vacuum with an accelerating voltage of 7.00 kV and a working distance of 4.7 mm. An InLens detector was used to collect images. Energy-dispersive X-ray spectroscopy (EDX) imaging was performed by using a Bruker

XFlash 5010 EDX detector with 123 eV resolution. Nearly 5 mg of preactivated sample was placed on a carbon tape for each measurement and coated by gold. The remaining IL-MOF composites were imaged using Zeiss Ultra Plus microscope and InLens detector. Images were obtained employing 7.00 kV accelerating voltage for the rest of the samples except [(EtO)₂IM][NTf₂]/ZIF-8 where 5 kV voltage was applied to avoid charging.

3.2.4 Brunauer–Emmett–Teller (BET) Surface Area

Brunauer-Emmett-Teller (BET) isotherm^[70] was used to determine the specific surface area of powders and porous solids. In the BET isotherm, binding energy of second layer is taken into consideration as shown in following equation:

$$\theta = \frac{pp_0(T)}{\left[p_0(T) + p - p \exp\left(\frac{\varepsilon' - \varepsilon}{k_B T}\right) \right] \left[p_0(T) - p \exp\left(\frac{\varepsilon' - \varepsilon}{k_B T}\right) \right]} \quad (3.1)$$

where θ is coverage, p is pressure, p_0 is ambient pressure, T is temperature, ε and ε' are the binding energy of first and second layers, respectively.

More common representation of BET isotherm is given in the following equation:

$$\frac{p}{n^a(p^o - p)} = \frac{1}{n_a^m} + \frac{C-1}{n_a^m C} \frac{p}{p^o} \quad (3.2)$$

where n^a is the amount adsorbed at a certain relative pressure, n_a^m is the monolayer capacity and C is constant. A plot of $p/n^a(p^o - p)$ versus p/p^o gives a slope of $(C-1)/n_a^m C$ and intercept of $1/n_a^m$ within a certain relative pressure range.

3.2.5 Infrared Spectroscopy

FTIR measurements were performed on a Thermo Scientific Nicolet iS10 and Bruker Vertex 80v IR spectrometers. For pristine ZIF-8, bulk [BMIM][BF₄], and [BMIM][BF₄]/ZIF-8 samples a platinum diamond attenuated total reflection (ATR) cell was used in Thermo Scientific Nicolet iS10. Spectra were collected at a spectral resolution of 2 cm⁻¹ in a range of

500-4000 cm⁻¹ in air at room temperature. For each spectrum 512 sample scans were collected and averaged, an average of 64 background scans was subtracted. The rest of the composites and bulk ILs were measured with the same scan numbers and within the same resolution range using KBr cell in Bruker Vertex 80v IR spectrometer. Deconvolution of IR bands were performed on Fityk^[71] software by using Voigt function.

3.2.6 Elemental Analysis

For the quantification of IL loading in the pores of MOF, elemental analysis was carried for each composite. For [BMIM][BF₄]/ZIF-8 samples, Inductively Coupled Plasma Mass Spectrometry (ICP-MS) was used. An Agilent 7700x ICP-MS (Agilent Technologies Inc., Tokyo, Japan) was used for the quantification of boron and zinc atoms in each IL-incorporated ZIF-8 sample. Samples for each measurement were prepared by dissolving 50 mg of [BMIM][BF₄]/ZIF-8 in 10 ml of 37 wt% HCl. The ICP-MS was operated with a PFA concentric nebulizer, an inert sample introduction kit with a sapphire injector (inner diameter 2.5 mm, for Agilent 7700 series, Agilent Technologies, Germany) and Ni sampler/skimmer cones. Spex Certiprep Multi-element calibration standards were followed for the preparation of external calibration solutions. 1 µg/L tuning solution was used for instrumental optimizations. Calculations of the analytical results were performed by MassHunter software. Elemental analyses of the samples given in the second part of the thesis were carried out by X-Ray Fluorescence. Bruker S8 Tiger XRF spectrometer was used with mylar film under helium atmosphere.

3.3 High Pressure Volumetric Adsorption Analysis

Gas adsorption measurements were performed using High Pressure Volumetric Analyzer (HPVA) II -200. Nearly 0.45 g of each sample was filled into a sample holder and activated in the degas port overnight at 10–3 mbar, 125 °C. After the activation period, the sample holder was assembled in the analysis port, and the system was purged before the analysis. Adsorption isotherms were acquired up to 10 bar for all gases. Excess adsorption isotherms of CH₄ and N₂ gases were fitted to a dual-site Langmuir isotherm equation, and

that of CO₂ was fitted to a Freundlich model which are given in Equation 3.3 and Equation 3.4, respectively, for each sample. Selectivities of the samples were calculated by dividing the higher gas uptake by the lower one at the same pressure and temperature. For heat of adsorption measurements, adsorptions of CO₂, CH₄, and N₂ gases were measured at two different temperatures (10 and 25 °C) up to 2 bar. For the integration of enthalpy, the virial equation of state was used for the description of an adsorbed phase. Uptake values obtained from experiments were fitted to the virial-type thermal adsorption equation, which is shown in Equation 3.5 where N is uptake, P is pressure, T is temperature, and a_i and b_i are constants provided in Appendix A. The isosteric heat of adsorption (Q_{st}) values were calculated according to Equation 3.6 where R is the gas constant.

$$n = \frac{PA}{P+B} + \frac{PC}{P+D} \quad (3.3)$$

$$n = \frac{AP^C}{B+P^C} \quad (3.4)$$

$$\ln P = \ln N + \frac{1}{T} \sum_{i=0}^5 a_i N^i + \sum_{i=0}^3 b_i N^i \quad (3.5)$$

$$Q_{st} = -R \sum_{i=0}^5 a_i N^i \quad (3.6)$$

Chapter 4*

PREPARATION, CHARACTERIZATION, AND ADSORPTION MEASUREMENTS OF [BMIM][BF₄]/ZIF-8 SAMPLES

4.1 Preparation of [BMIM][BF₄]/ZIF-8 Samples

IL-incorporated MOF samples were prepared in the open atmosphere following the procedure explained in Chapter 3. In short, IL was dissolved in 30 ml of acetone and mixed for 15 minutes. Then ZIF-8 was added into the solution and kept mixing at 30 °C until acetone was evaporated. After the acetone was evaporated, residual was dried in oven at 105 °C overnight. 0.3, 0.2, and 0.05 g ILs and 0.7, 0.8, and 0.95 g ZIF-8 were used for 30 wt%, 20 wt%, and 5 wt%, respectively.

4.2 Characterization of ZIF-8, [BMIM][BF₄] and [BMIM][BF₄]/ZIF-8 Samples

4.2.1 Elemental Analysis

Once the [BMIM][BF₄]-incorporated ZIF-8 samples with different IL loadings were prepared, they were characterized in deep detail to i) confirm successful incorporation of ILs

*The results given in this chapter were published in The Journal of Physical Chemistry C with following reference: B. Koyuturk, C. Altintas, F. P. Kinik, S. Keskin, A. Uzun, *The Journal of Physical Chemistry C* **2017**, *121*, 10370-10381. The original manuscript has been rearranged to conform to the format requirements of the dissertation.

into ZIF-8 pores; ii) check whether the framework of ZIF-8 remains intact upon IL incorporation; and iii) elucidate any interactions between IL and ZIF-8. For this purpose, the ICP-MS analysis of each sample was first performed to quantify the amounts of boron and zinc atoms in IL/MOF samples. The results obtained are listed in Table 4.1. Based on the ratio of boron and zinc atom concentrations and on the stoichiometry of ZIF-8 (C₈H₁₀N₄Zn), the respective IL loadings were determined as 3.8, 20, and 28.3 wt% for samples prepared by using 5, 20, 30 wt% IL, respectively. According to these results, the samples were labeled as IL₄/ZIF-8, IL₂₀/ZIF-8, and IL₂₈/ZIF-8, respectively, where the numbers in subscripts provide the loading amount of [BMIM][BF₄] in wt% as determined by ICP-MS (Table 4.1).

Table 4.1: Boron and zinc amounts in IL-incorporated ZIF-8 samples determined by ICP-MS.

Sample	Boron (ppb)	Zinc (ppb)	Measured IL loading (wt%)	Expected IL loading from synthesis amounts (wt%)
IL ₄ /ZIF-8	10550	1590959	3.8	5
IL ₂₀ /ZIF-8	45001	1078315	20	20
IL ₂₈ /ZIF-8	55337	83972	28.3	30

4.2.2 Scanning Electron Microscopy (SEM)

Figure 4.1 illustrates representative SEM images for each of IL-incorporated ZIF-8 samples, IL₄/ZIF-8, IL₂₀/ZIF-8, and IL₂₈/ZIF-8, in comparison with that of pristine ZIF-8. Images indicate that the framework of ZIF-8 remains intact upon the incorporation of IL at each loading considered. Moreover, EDX analysis performed on these images, as shown on a representative sample, IL₂₈/ZIF-8, in Figure 4.2, confirms the uniform distribution of IL evidenced by the dispersion of fluorine atoms.

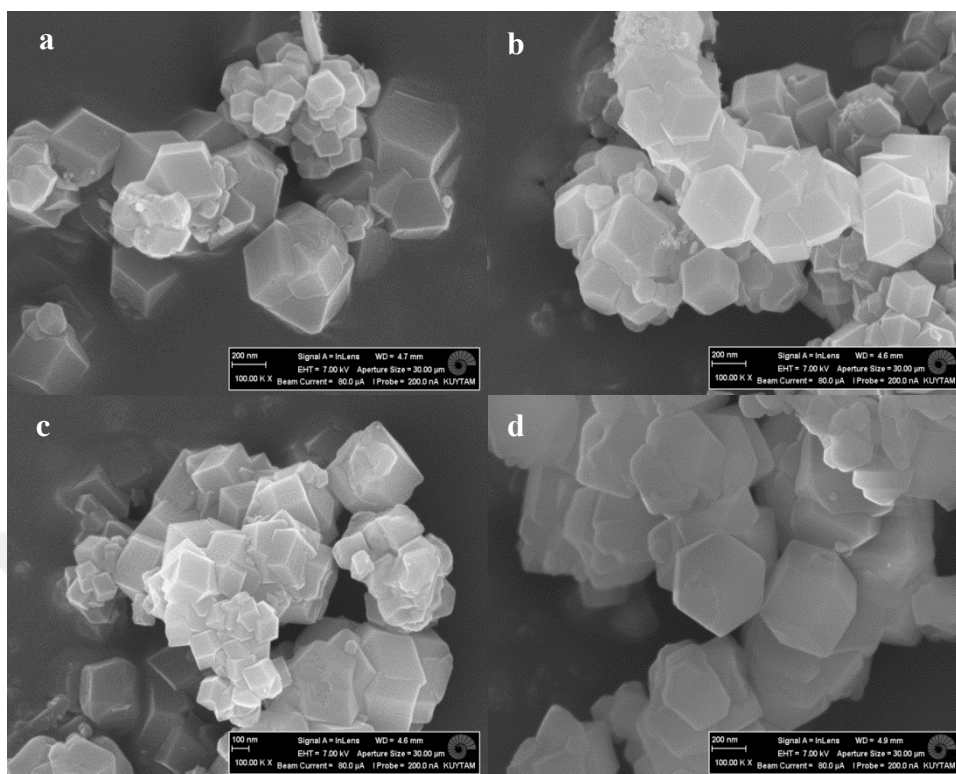


Figure 4.1: SEM images of ZIF-8 and [BMIM][BF₄]/ZIF-8 samples at 100 K \times magnification: (a) ZIF-8, (b) IL₄/ZIF-8, (c) IL₂₀/ZIF-8, and (d) IL₂₈/ZIF-8.

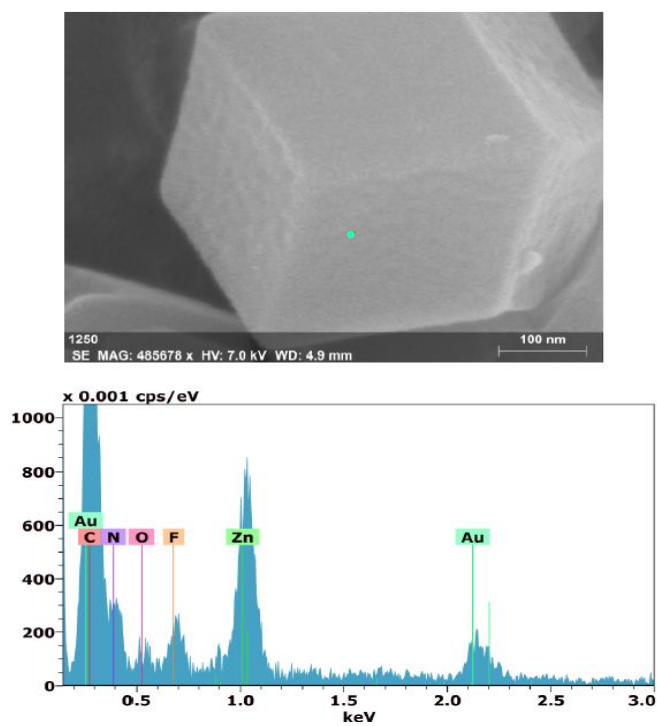


Figure 4.2: EDX results on IL₂₈/ZIF-8.

4.2.3 Powder X-Ray Diffraction (PXRD)

Powder X-Ray Diffraction experiments were conducted to understand the changes in the crystal structure of ZIF-8 upon IL incorporation. Once we found XRD pattern of pristine ZIF-8 consistent with the previous works in the literature^[72], IL-incorporated ZIF-8 samples were measured and concluded that the crystalline structure of ZIF-8 remained intact upon IL incorporation up to 30 wt% as shown in Figure 4.3. This observation is consistent with the SEM images (Figure 4.1) indicating the topology of MOF remained unchanged upon the IL incorporation.

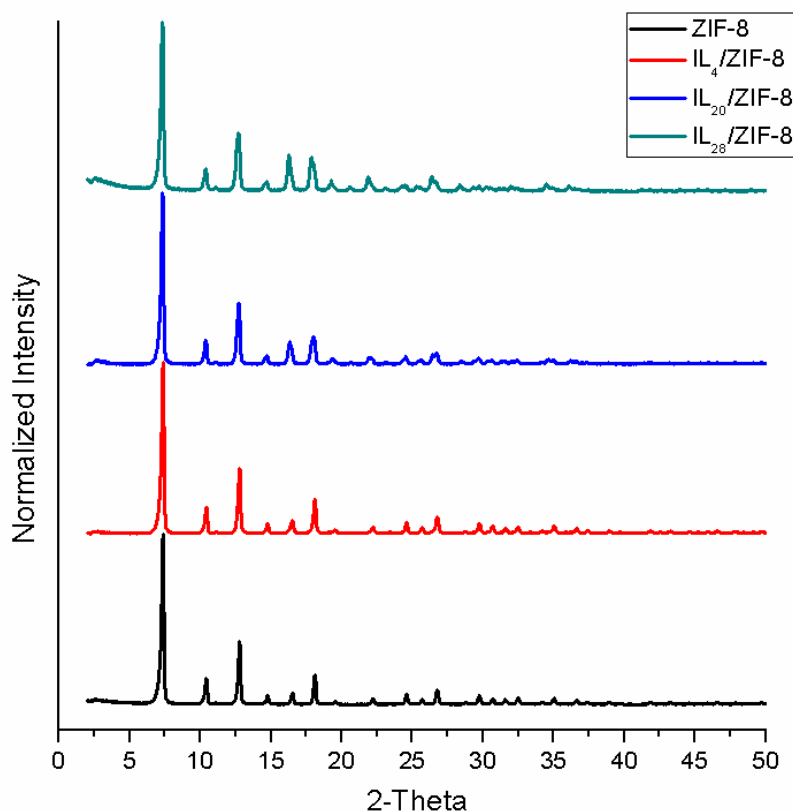


Figure 4.3: XRD patterns of ZIF-8 (black) and [BMIM][BF₄]/ZIF-8 samples: IL₄/ZIF-8 (red), IL₂₀/ZIF-8 (blue), and IL₂₈/ZIF-8 (green).

4.2.4 Brunauer–Emmett–Teller (BET) Surface Area

BET results support these observations and show that surface area and pore volume of ZIF-8 decrease with increased IL loading from 1617 m²/g (consistent with the literature^[73]) and 0.669 cm³/g to 1207, 725, 177 m²/g and to 0.502, 0.318, 0.112 cm³/g for IL₄/ZIF-8, IL₂₀/ZIF-8, and IL₂₈/ZIF-8, respectively. Not surprisingly, incorporation of IL into the pores of MOF caused a decrease in the surface area and pore volume of ZIF-8 as illustrated in N₂ adsorption isotherms at 77 K given in Figure 4.4 and in Table 4.2. Pore volume and surface area are found to be correlated with the IL loading, as shown in Appendix B.

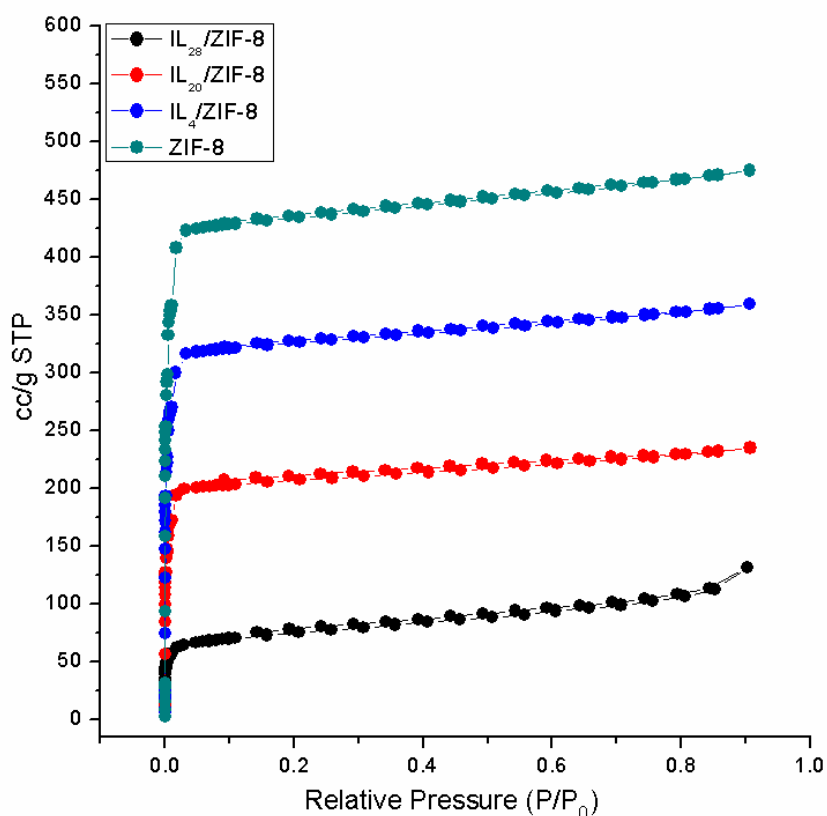


Figure 4.4: N₂ isotherms of ZIF-8 and [BMIM][BF₄]/ZIF-8 samples at 77 K.

Table 4. 2: Measured BET surface areas and pore volumes of ZIF-8 and [BMIM][BF₄]/ZIF-8.

Sample	S _{BET} (m ² /g)	Pore volume (cm ³ /g)
ZIF-8	1617	0.669
IL ₄ /ZIF-8	1207	0.502
IL ₂₀ /ZIF-8	725	0.318
IL ₂₈ /ZIF-8	177	0.112

4.2.5 Thermal Gravimetric Analysis (TGA)

TGA measurements performed on these samples revealed that incorporation of [BMIM][BF₄] into ZIF-8 leads to a substantial change in the thermal stability of both ZIF-8 and bulk IL as illustrated in Figures 4.5 and 4.6, and in Table 4.3. Accordingly, the pristine ZIF-8 and bulk [BMIM][BF₄] in liquid form start to decompose at 375 and 314 °C, respectively. However, when the IL was incorporated into MOF, its decomposition temperature decreases by more than 50 °C. Such decrease in thermal stability limit of IL was also observed when different ILs were supported on various metal oxides.^[74-75] Similar to the case in [BMIM][PF₆] incorporated ZIF-8,^[33] this decrease in the thermal stability limit indicates direct interactions between IL and MOF. These interactions were also evidenced by the remaining sample weight at the end of the TGA measurements. Data show that the bulk IL completely disappears before temperature reaches to 450 °C. At this temperature pristine ZIF-8 loses approximately 5 wt% of its initial weight. Based on these values one would expect to have approximately 70 wt% of the initial mass (assuming all of IL leaves the sample and remaining ZIF-8 portion of the sample loses only 5 wt% of the initial mass) remaining on IL₂₈/ZIF-8 sample at 450 °C. However, data given in Figure 5 show that only 60 wt% of IL₂₈/ZIF-8 remains at this temperature. These results illustrate that when the IL is decomposing and leaving the MOF, it also removes some portion of the MOF as well, indicating the presence of direct interactions between IL and MOF, affecting the thermal decomposition mechanism.

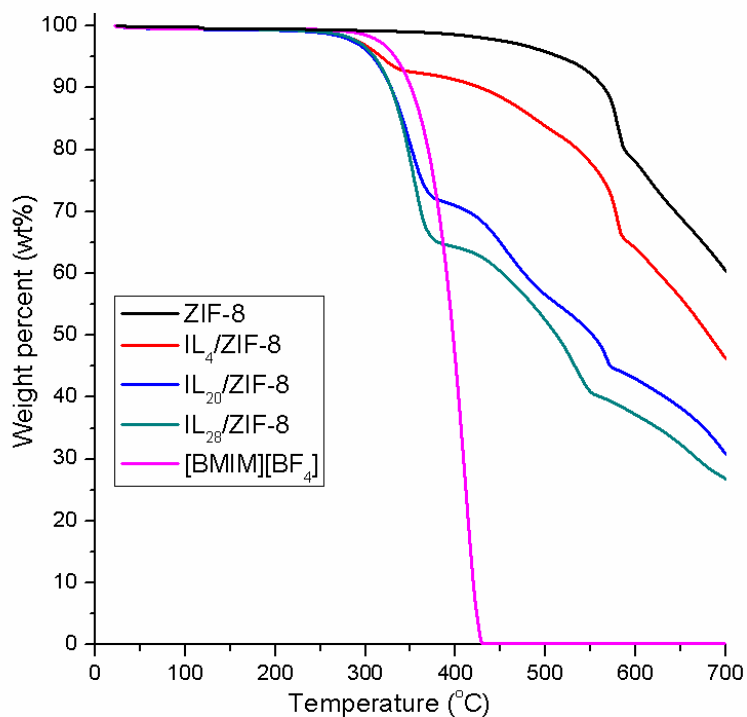


Figure 4.5: Thermal stability of pristine ZIF-8, bulk [BMIM][BF₄], and IL-incorporated samples.

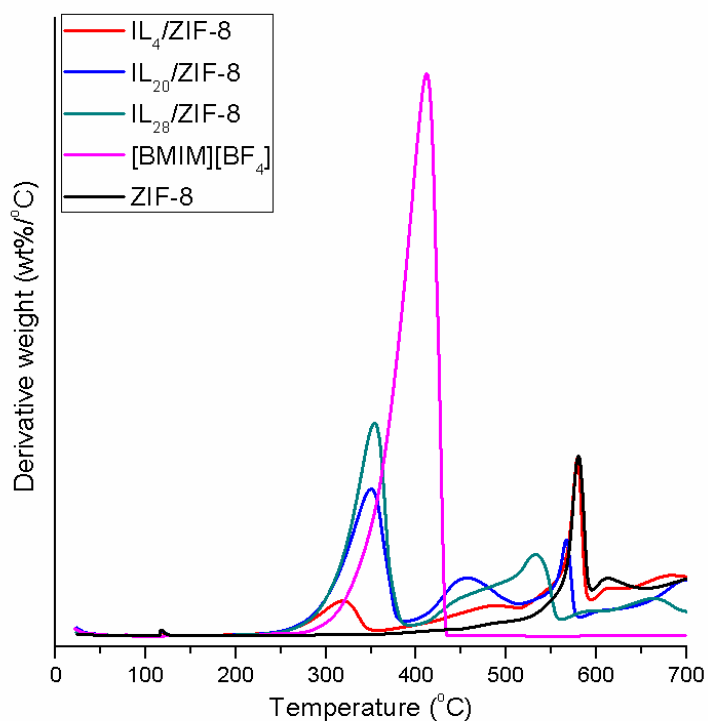


Figure 4.6: Derivative weight change of ZIF-8 and IL/ZIF-8 samples.

Table 4.3: Derivative decomposition temperature (T'_{onset} ^[76]) of bulk [BMIM][BF₄], pristine ZIF-8, and [BMIM][BF₄]/ZIF-8 samples.

Sample	T'_{onset} (°C)
ZIF-8	375
[BMIM][BF ₄]	314
IL ₄ /ZIF-8	250
IL ₂₀ /ZIF-8	268
IL ₂₈ /ZIF-8	274

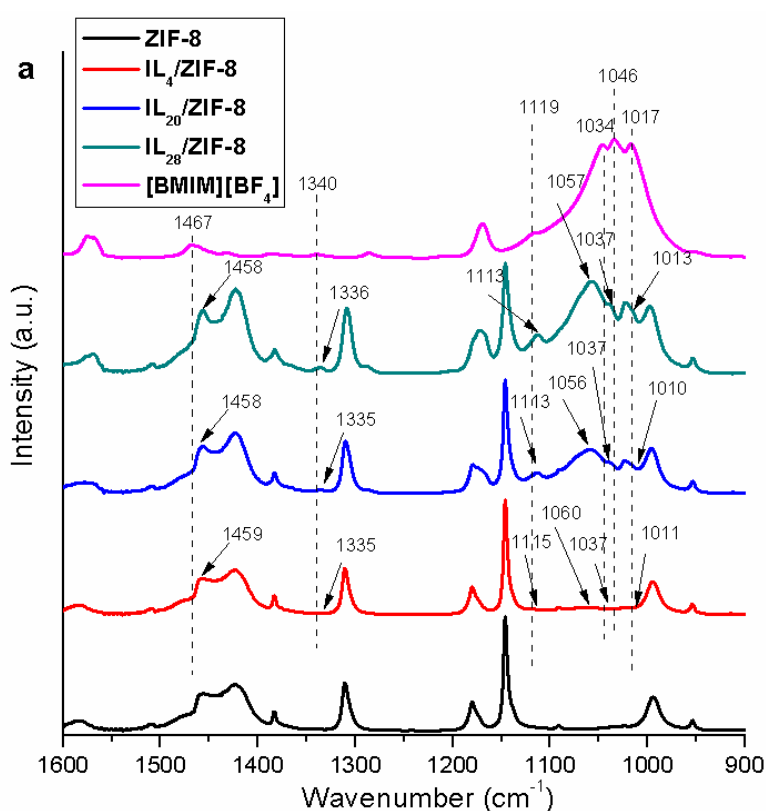
4.2.6 Infrared (IR) Spectroscopy

Aiming at elucidating these interactions, we focused on identifying any changes in the positions of IR bands of bulk IL upon its incorporation into the MOF. Figure 4.7 presents the corresponding IR spectra of bulk IL, ZIF-8, and IL/ZIF-8 samples prepared at different IL loadings. Assignment of the IR features was done based on a previous study performed on the same IL coating on various metal oxides.^[76] Figure 4.7 provides the IR data in two different frequency regions: a) 1600-900 cm⁻¹ and b) 3200-2800 cm⁻¹. IR features observed on these spectra were analyzed in detail: first the peaks were deconvoluted then the shifts in band positions were determined by considering the corresponding positions in bulk IL as reference. These shifts are summarized in Table 4.4 and Table 4.5 for high and low wavenumber regions, respectively.

Deconvoluted IR spectra of [BMIM][BF₄], ZIF-8, and [BMIM][BF₄]/ZIF-8 at three different IL loadings are given in Appendix C.^[77] The most intense bands of [BF₄]⁻ anion are present in the region between 1600-900 cm⁻¹. In this region data indicate that some of the main IR features of bulk IL show changes in their positions and intensities upon IL incorporation into the MOF. These changes complement the TGA results and confirm that there are interactions between IL and MOF.^[32-33] Accordingly, six of the main IR features in this region show major shifts from their counterparts in the spectrum of bulk [BMIM][BF₄]. The band at 987 cm⁻¹ assigned to butyl $\delta(\text{HC1H})$ rocking shifts to 978, 979, and 981 cm⁻¹ on IL₄/ZIF-8, IL₂₀/ZIF-8 and IL₂₈/ZIF-8, respectively. Similarly, the band at 1340 cm⁻¹ attributed

to butyl $\delta(\text{C1H})$, $\delta(\text{C2H})$, and $\delta(\text{C3H})$ and *n*-butyl stretching in cation indicated red shifts of -4, -5, and -5 cm^{-1} on IL₄/ZIF-8, IL₂₀/ZIF-8, and IL₂₈/ZIF-8, respectively. Likewise, the band at 1017 cm^{-1} , assigned to butyl $\delta(\text{HC4H})$ (or $\nu(\text{BF}_4)_{\text{asym}}$), shifts by -6, -7, and -4 cm^{-1} , while that at 1574 cm^{-1} attributed to $\nu(\text{C2-N})$ exhibiting a blue shift of 3, 3, and 20 cm^{-1} on IL₄/ZIF-8, IL₂₀/ZIF-8, and IL₂₈/ZIF-8, respectively, possibly due to a decrease in the bond energy between imidazolium ring and butyl group in cation. Moreover, the band at 1119 cm^{-1} assigned to $\delta(\text{C2H})$, $\delta(\text{C4H})$, and $\delta(\text{C5H})$ on the imidazolium ring exhibits weak red shifts slightly larger than our spectral resolution ($>2 \text{ cm}^{-1}$) resulting from the strengthening of the C2-N bond. The corresponding shifts were -4, -6, and -6 cm^{-1} , for IL₄/ZIF-8, IL₂₀/ZIF-8 and IL₂₈/ZIF-8, respectively. Another peak at 1467 cm^{-1} assigned to ring $\delta(\text{CH}_3)$ wagging shows red shifts of -8, -9, and -9 cm^{-1} for IL₄/ZIF-8, IL₂₀/ZIF-8, and IL₂₈/ZIF-8, respectively. The remaining bands in the low frequency region were 1034 and 1046 cm^{-1} attributed to $\nu(\text{BF}_4)_{\text{asym}}$. For each IL loading considered, the former one shifts to 1037 cm^{-1} (this shift amount might be within the error range, considering the spectral resolution was 2 cm^{-1}). The latter one, on the other hand, illustrates considerably high blue shifts of 14, 10, and 11 cm^{-1} on IL₄/ZIF-8, IL₂₀/ZIF-8, and IL₂₈/ZIF-8, respectively. Similar to the changes in the band positions in lower region, bands in high wavenumber region also present shifts in their positions. Bands at 2939 and 3113 cm^{-1} assigned to ring $\nu(\text{CH}_3)_{\text{sym}}$ and ring $\nu(\text{CH}_3)_{\text{asym}}$ are two of these bands. The ring $\nu(\text{CH}_3)_{\text{sym}}$ exhibits red shifts of -9, -7, and -9 cm^{-1} on IL₄/ZIF-8, IL₂₀/ZIF-8, and IL₂₈/ZIF-8, respectively, and the ring $\nu(\text{CH}_3)_{\text{asym}}$ shows a red shift of -16 cm^{-1} on each IL/ZIF-8 samples. These red shifts indicate a weakening in the interaction between ring and methyl group in cation. The latter one in high frequency region (3121 cm^{-1}) assigned to $\nu(\text{C2H})_{\text{sym}}$ on the ring shows the most significant shift on each sample; a blue shift of 26, 27, and 26 cm^{-1} for IL₄/ZIF-8, IL₂₀/ZIF-8, and IL₂₈/ZIF-8, respectively. These changes in the band positions can be interpreted in different ways. However, based on the findings of a previous study,^[76] we interpret the interactions of ZIF-8 with the IL as described in the following: Due to the presence of imidazolium ring in ZIF-8, anion of IL interacts with MOF and receives electrons. This interaction lead to an increase in inner B-F bond strength, indicated by blue shifts in $\nu(\text{BF}_4)_{\text{asym}}$. As anion prefers to interact more with the MOF, its interionic interactions weakens consistently with an increase in C2-H stretching in imidazolium ring.^[74-75] This change also leads to an increase in the electron density of cation and corresponding strengthening of the inner bonds in imidazolium ring. Stronger inner

bonds can also be originated by the presence of hydrogen bonding between framework and cation. Also the assignment of the IR features in bulk IL spectrum was done based on a DFT-based study reporting the most stable conformer of [BMIM][BF₄],^[76] however ILs may have more than one stable conformer and depending on the conformers preferred inside the MOF cage, there may be different shifts observed in IR features. It is suggested that detailed DFT-based studies can provide valuable information in the way of elucidating these interactions between the ILs and MOFs in such IL-incorporated MOF materials.^[33]



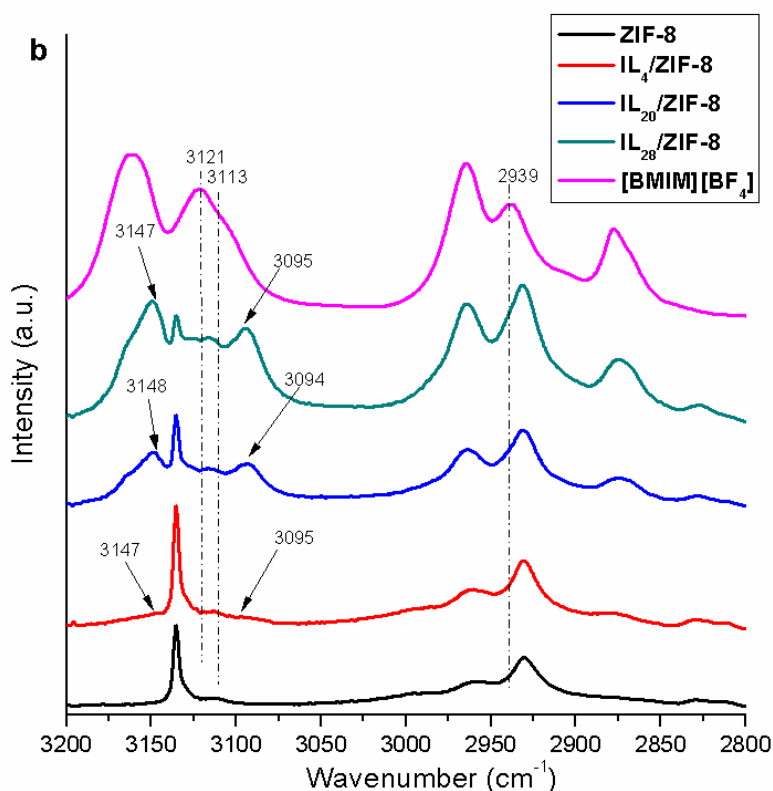


Figure 4.7: IR spectra of IL-incorporated MOFs, bulk [BMIM][BF₄] and pristine ZIF-8: (a) 900-1600 cm⁻¹, (b) 2800-3200 cm⁻¹.

Table 4. 4: Shifts in IR bands of [BMIM][BF₄] in the lower region.

IL-incorporated MOF	IR bands of bulk [BMIM][BF ₄] in lower frequency region (cm ⁻¹)										
	987	1017	1034	1046	1119	1170	1285	1340	1385	1467	1574
IL ₄ /ZIF-8	-9	-6	3	14	-4	0	3	-5	0	-8	20
IL ₂₀ /ZIF-8	-8	-7	3	10	-6	0	3	-5	0	-9	3
IL ₂₈ /ZIF-8	-6	-4	3	11	-6	0	3	-4	0	-9	3

Table 4. 5: Shifts in IR bands of [BMIM][BF₄] in the higher region.

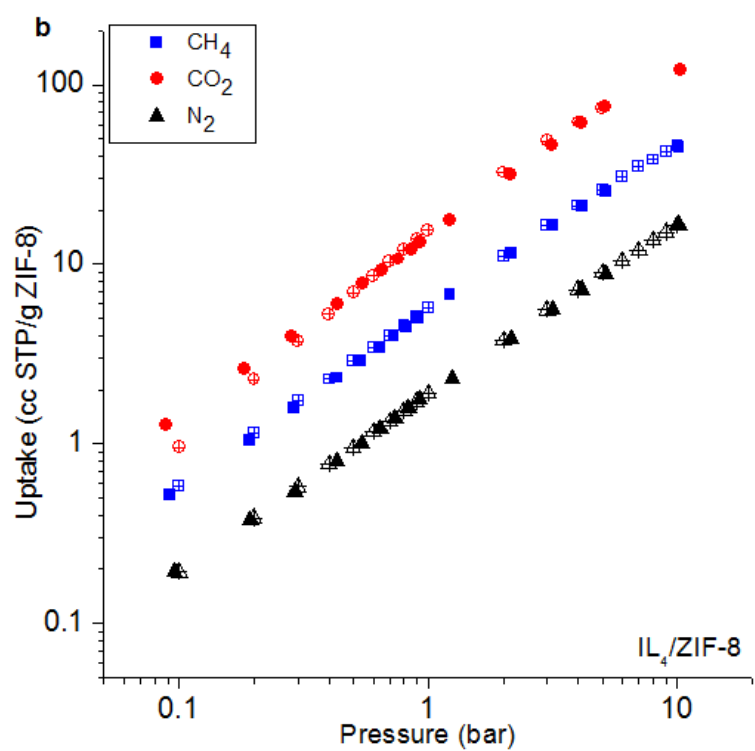
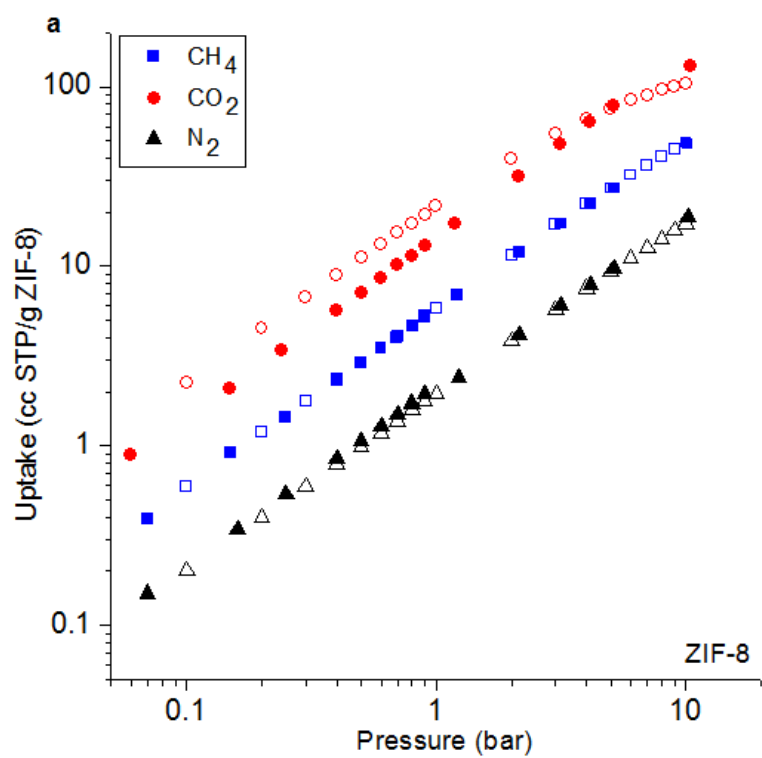
IL-incorporated MOF	IR bands of bulk [BMIM][BF ₄] in higher frequency region (cm ⁻¹)					
	2876	2939	2964	3113	3121	3162
IL ₄ /ZIF-8	-1	-9	-2	19	26	-1
IL ₂₀ /ZIF-8	-3	-7	-1	19	27	1
IL ₂₈ /ZIF-8	-1	-9	0	19	26	1

4.3 Performance Measurements

In the performance measurements section, gas uptakes and ideal selectivity of composites are given and compared with the performance of pristine ZIF-8.

4.3.1 Gas Adsorption Analysis of ZIF-8

As discussed above, detailed characterization of the samples prepared by the incorporation of [BMIM][BF₄] into ZIF-8 provides direct evidence on the presence of interactions between anion of the IL and ZIF-8. These interactions can have a significant effect on the gas adsorption and separation performance of pure ZIF-8. Aiming at revealing the consequences of these interactions, volumetric gas adsorption experiments were carried out for CH₄, N₂, and CO₂ in a pressure range of 0.1-10 bar at 298 K. Single-component gas adsorption isotherms of CH₄ and N₂ were fitted to the dual site Langmuir model whereas CO₂ uptakes were fitted to the Freundlich model. Experimental measurements on pristine ZIF-8 provide consistent data with the literature.^[25] Parameters of these models are provided in Appendix A. GCMC (Grand Canonical Monte Carlo) simulations which are molecular simulations used to predict adsorption properties of various materials were also performed by collaborative work for each gas in the same pressure range and at the same temperature to complement the experimental measurements. Gas uptake results of experiments and simulations per gram of MOF measured up to 10 bar for the pristine MOF and IL/MOF samples with different IL loadings are given in Figure 4.8.



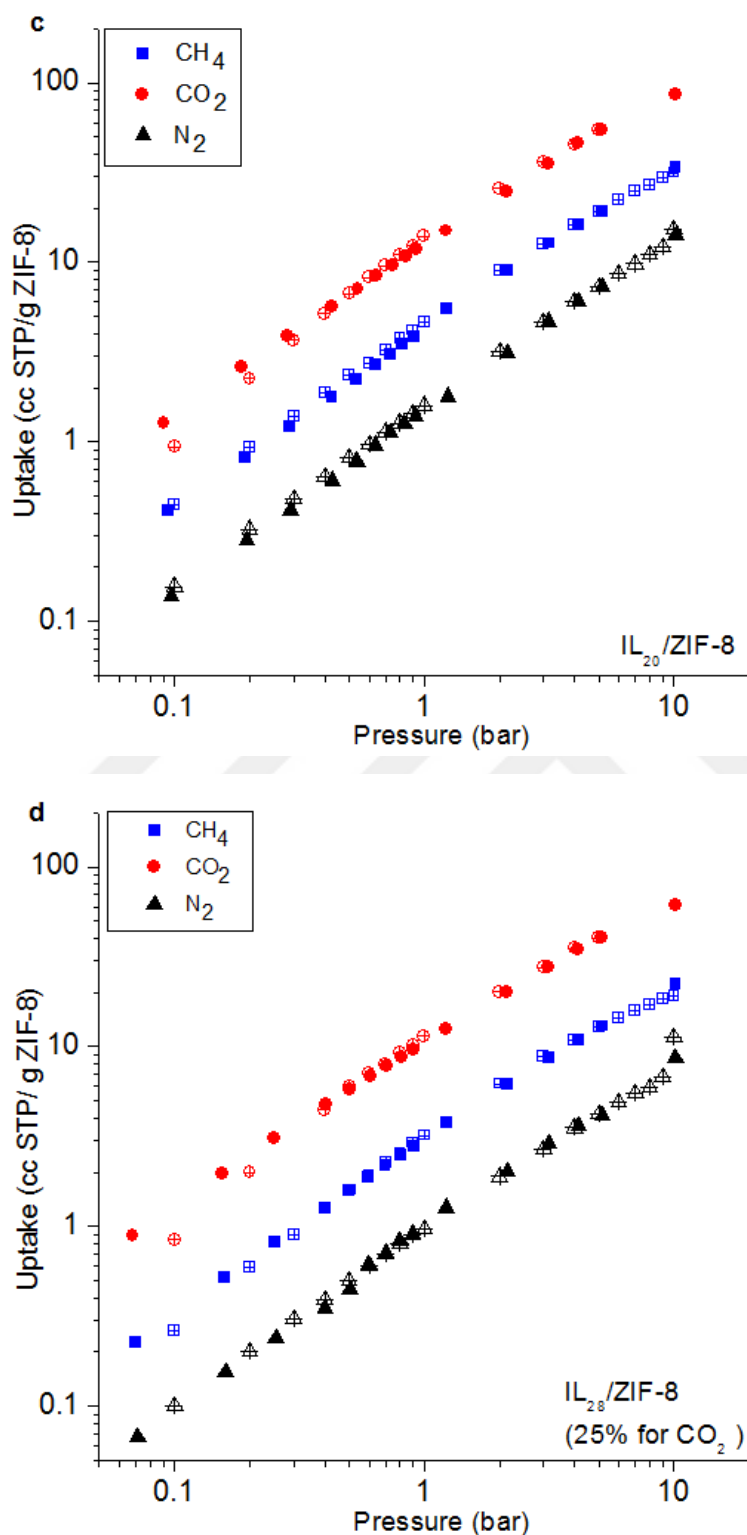


Figure 4.8: Gas uptakes of ZIF-8 and IL-incorporated ZIF-8 obtained from experiments and simulations: (a) ZIF-8, (b) IL₄/ZIF-8, (c) IL₂₀/ZIF-8, (d) IL₂₈/ZIF-8. Filled symbols: experimental uptake values, empty symbols: simulated uptake values multiplied with the factors.

Figure 4.8 shows that simulations agree well with the experimental gas uptake measurements. IL molecules were loaded into ZIF-8 cages with fixed loading amounts as determined by the ICP-MS measurements to maintain consistency for the GCMC calculations. However, because of the limitations originated from the force field (UFF) that was used for IL loading, a maximum IL amount of 25 wt% could be reached for CO₂. As illustrated above, there are interactions between MOF and IL molecules resulting in changes in electron densities on both MOF and IL. Thus, uptake values calculated for IL-incorporated ZIF-8 samples were multiplied by a pressure dependent factor (f). For comparison, unmodified simulation results are also given in Appendix D. Considering the values reported in Appendix D, the strongest modification of the simulated results was needed for the CO₂ uptake of IL/ZIF-8 samples. This result might imply that modification of the sites for gas adsorption by the incorporation of IL was more pronounced for the CO₂ adsorption, as we discussed further below.

In Figure 4.9, gas uptakes of IL-incorporated MOF samples were compared with their corresponding values of pristine ZIF-8. Uptake values for CH₄ and N₂ become lower throughout the entire pressure range upon the IL incorporation. However, the case is different with CO₂ on IL₂₀/ZIF-8, for which the uptake value becomes slightly higher than its counterpart on pristine ZIF-8 up to 0.2 bar. For instance, at 0.1 bar it reaches a maximum of approximately 108.6% of its counterpart in pristine ZIF-8. As the IL loading increased, a higher degree of decrease in uptakes is expected at high pressures because of a decrease in the available pore space of MOF as shown in Table 4.1. However, changes in the uptake behavior of IL/MOF samples for different gases specifically at low pressures cannot be simply described by a decrease in the available space of the framework. Interactions between the IL and MOF can either create new sites for gas adsorption or strongly modify the existing ones. This influence is more significant at low pressure, where the interactions between the adsorbates and adsorption sites is the dominant factor (not the available space) controlling the gas adsorption behavior.^[33]

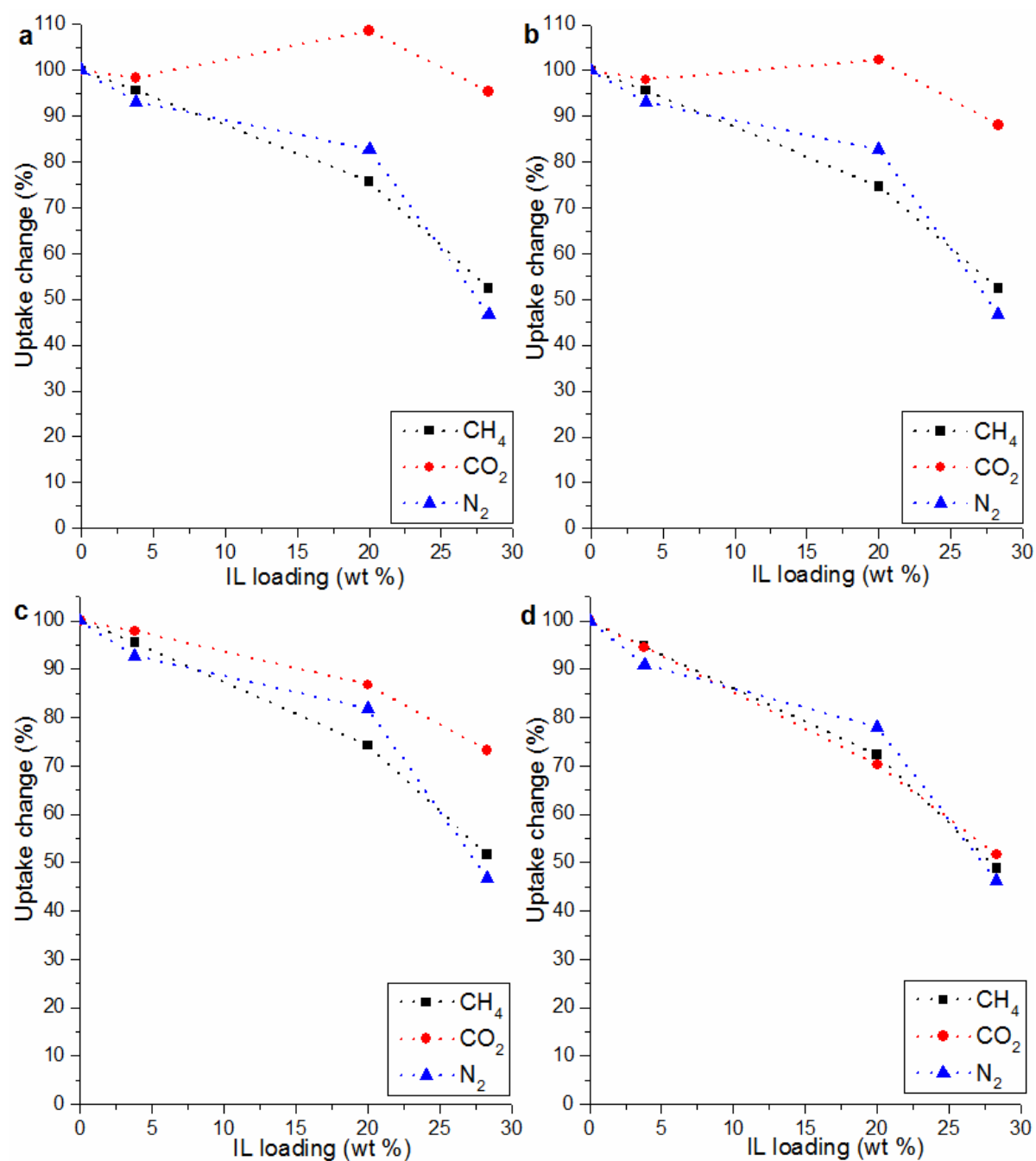
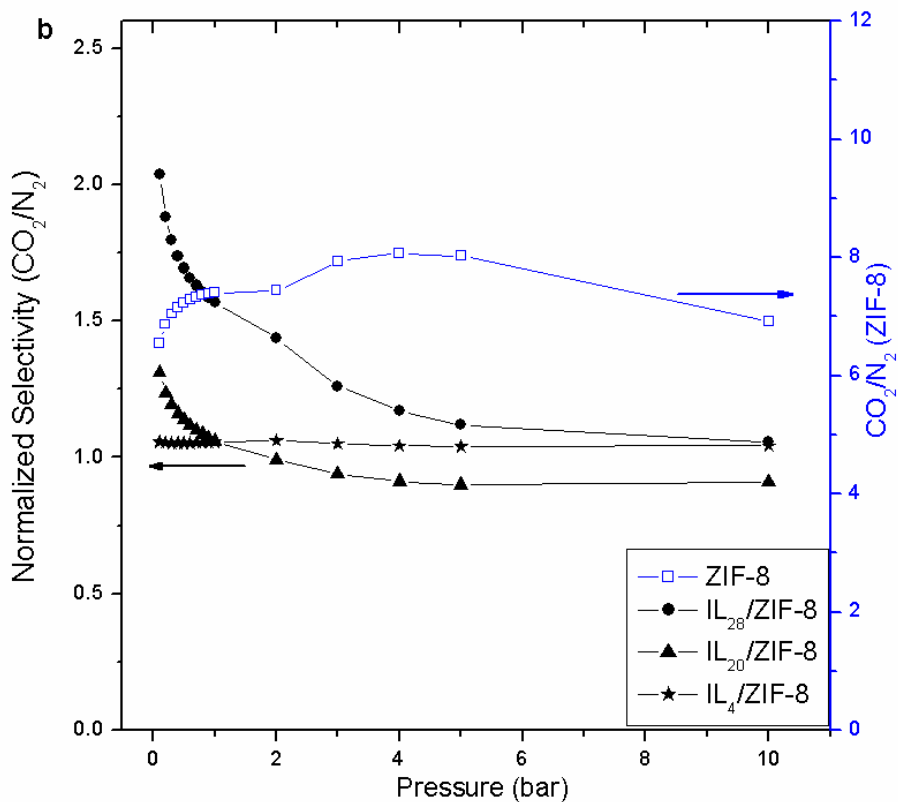
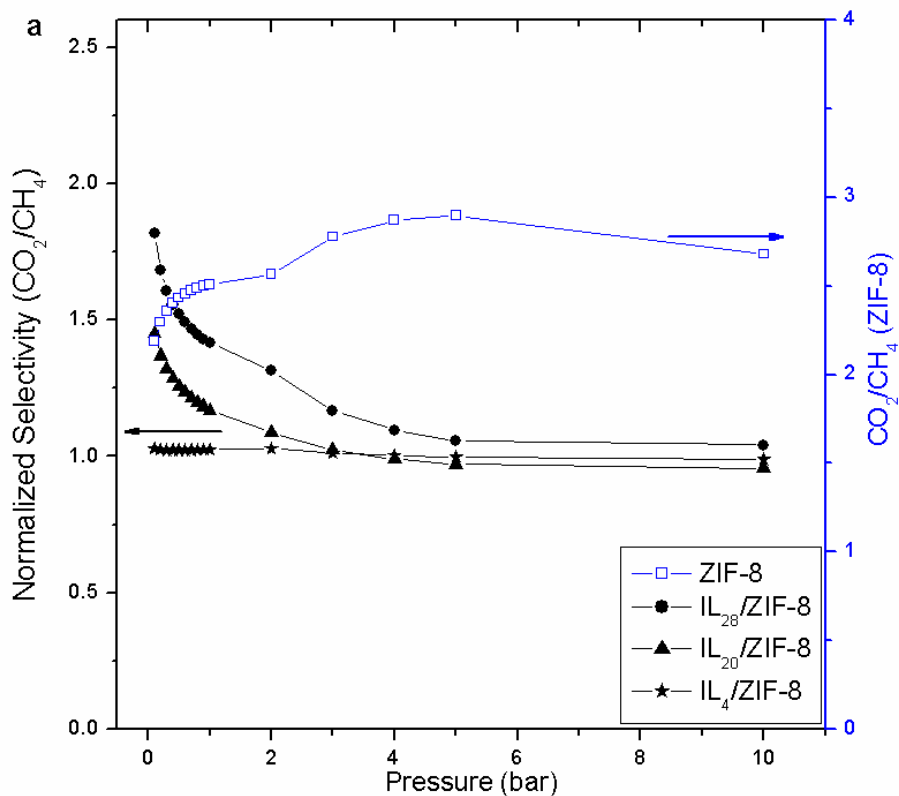


Figure 4.9: Uptake change (%) of CO₂, CH₄, and N₂ with respect to IL loading (wt%): (a) 0.1 bar, (b) 0.2 bar, (c) 1 bar, (d) 5 bar. Dotted lines are provided to guide the eye.

4.3.2 Selectivity Calculation and Comparison

Results in Figure 4.9 illustrate different degrees of changes on the uptakes of different gases in IL/MOF samples prepared with different IL amounts. These results suggest that the

gas separation performance of ZIF-8 can be tuned by incorporating ILs. To reveal the consequences of the changes in gas uptakes on the separation performance of the MOF, ideal gas selectivities of samples were calculated by dividing the higher gas uptake to lower one. Figure 4.10 shows that the ideal gas selectivities of IL-loaded ZIF-8 differ considerably from those observed on pristine ZIF-8. Relative selectivities calculated by normalizing the individual selectivities of IL-loaded samples to the corresponding selectivities of ZIF-8 are given in Figure 4.10. CO₂/CH₄, CO₂/N₂, and CH₄/N₂ selectivities of ZIF-8 and IL-loaded ZIF-8 samples are also shown in Appendix D. Data show that significant improvements were obtained especially for IL₂₈/ZIF-8. According to Figure 4.10(a), IL₂₈/ZIF-8 exhibits approximately 1.8 times higher CO₂/CH₄ selectivity than that of pristine ZIF-8 at 0.1 bar. Data also indicate that as the IL loading decreases, CO₂/CH₄ selectivity of IL-loaded sample approaches to the selectivity of ZIF-8. Higher separation performances observed at low pressures can be attributed to the higher electrostatic interactions between CO₂ and IL-incorporated MOF samples. The best performances of IL-incorporated MOF samples were observed for CO₂/N₂ selectivities of IL₂₀/ZIF-8 and IL₂₈/ZIF-8. At 0.1 bar, it reached to 2 and 1.3 times of the corresponding values of pristine ZIF-8, respectively. Among all samples considered with different IL loadings, only IL₂₀/ZIF-8 underperformed CH₄/N₂ selectivity of ZIF-8. CH₄/N₂ selectivities of IL₂₈/ZIF-8 and IL₄/ZIF-8 samples slightly surpass the selectivity of pure ZIF-8, since the difference between the amount of decrease in CH₄ and N₂ uptakes is lower than the other pairs.



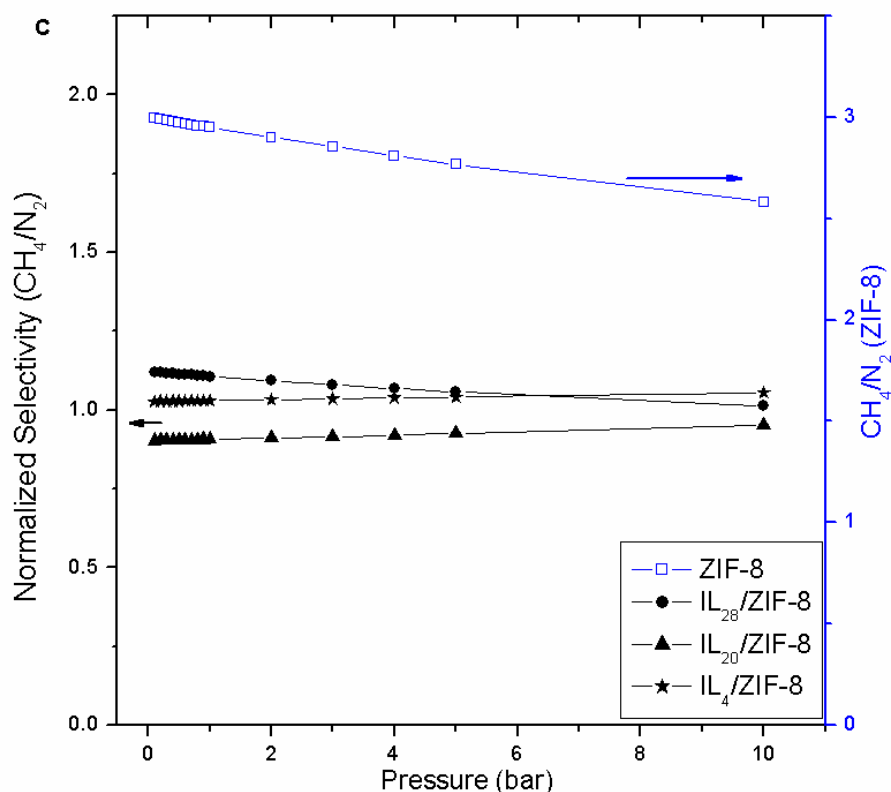


Figure 4.10: Normalized selectivities of samples (the ratio of IL/ZIF-8 samples to the selectivity of pure ZIF-8) for (a) CO₂/CH₄, (b) CO₂/N₂, (c) CH₄/N₂ separations.

The normalized selectivities of IL₂₈/ZIF-8 were compared with the normalized selectivities of [BMIM][BF₄]/Cu-BTC^[32] and [BMIM][PF₆]/ZIF-8^[33] that we previously studied and results given in Table 4.6. CO₂/CH₄ selectivity of the [BMIM][BF₄]/Cu-BTC sample was found to be lower than its counterpart on the pristine Cu-BTC, whereas the incorporation of the same IL into ZIF-8 leads to an improvement in the CO₂/CH₄ selectivity, specifically at low pressures. Similarly, CO₂/N₂ selectivity was more than doubled when [BMIM][PF₆] was incorporated into ZIF-8, while it leads to a slight decrease in the selectivity of the same gas pair when loaded in Cu-BTC. These results indicate that the type of MOF plays a major role in determining the separation performance of the IL/MOF sample even though the same IL is considered. The same case is also valid for the type of IL. When two different samples were prepared with the same MOF using different ILs (such as [BMIM][PF₆]- and [BMIM][BF₄]-incorporated ZIF-8 samples), the separation performance varies significantly by the change in IL type. For instance, [BMIM][PF₆] incorporation into ZIF-8 could not improve CH₄/N₂ selectivity, however [BMIM][BF₄] incorporation into ZIF-8

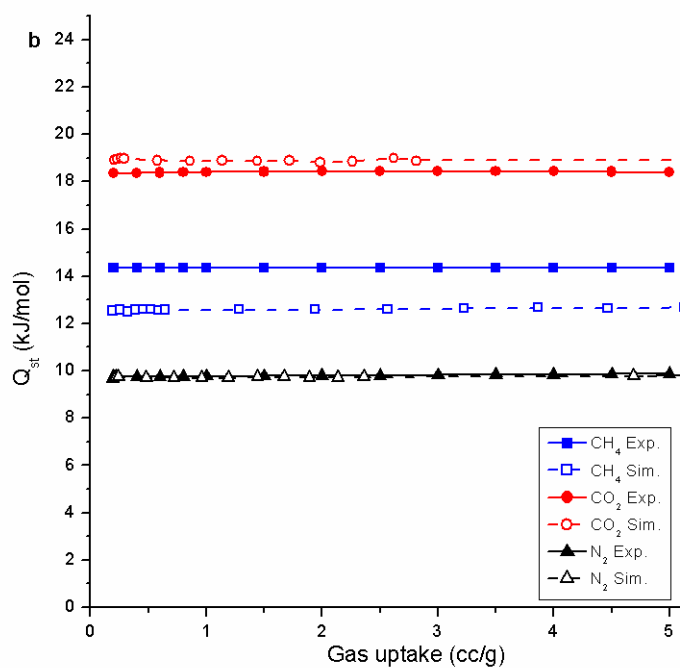
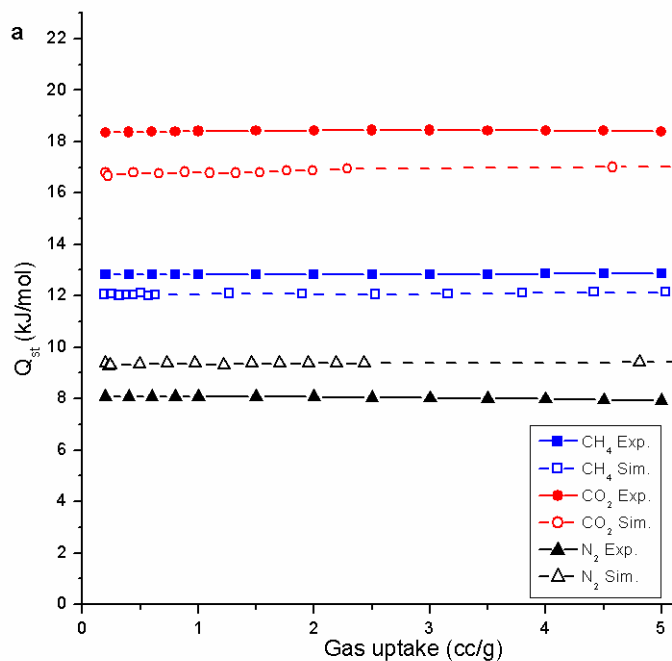
outperforms the performance of pristine ZIF-8 as a result of the interactions discussed above. These results and our ongoing studies illustrate that different combinations of IL-MOF pairs lead to different separation performances as they do not interact in the same way. Thus, we infer that each IL-MOF pair requires a separate investigation focusing on the elucidation of interactions and their consequences on the performance. Investigations on the effects of systematic changes in the structures of IL and MOF would add a significant value for the rational design of such novel materials with exceptional separation performance.

Table 4.6: Comparison of normalized selectivities of [BMIM][BF₄]/ZIF-8 with the normalized selectivities of other IL/MOF samples studied in our previous works.^[32-33] IL loading in MOFs are 30, 26 and 28 wt% for [BMIM][BF₄]/Cu-BTC, [BMIM][PF₆]/ZIF-8, and [BMIM][BF₄]/ZIF-8, respectively.

Selectivities	[BMIM][BF ₄]/Cu-BTC ^[32]			[BMIM][PF ₆]/ZIF-8 ^[33]			[BMIM][BF ₄]/ZIF-8		
	Pressure (bar)			Pressure (bar)			Pressure (bar)		
	0.1	0.5	1	0.1	0.5	1	0.1	0.5	1
CO ₂ /CH ₄	0.69	0.64	0.64	4.08	2.54	2.02	1.82	1.52	1.42
CO ₂ /N ₂	1.09	0.84	0.73	3.70	2.27	1.79	2.04	1.69	1.57
CH ₄ /N ₂	1.56	1.30	1.15	0.91	0.90	0.88	1.12	1.11	1.11

4.4 Heat of Adsorption Measurements

Aiming at revealing the reasons for improvements in selectivities as shown in Figure 4.10, isosteric heat of adsorption (Q_{st}) values for each gas on pristine ZIF-8, IL₄/ZIF-8, IL₂₀/ZIF-8, and IL₂₈/ZIF-8 were measured. Q_{st} values of CO₂, CH₄, and N₂ adsorbed on ZIF-8, shown in Figure 4.11, are consistent with the literature.^[78] Data show that the Q_{st} of CO₂ significantly increased from approximately 18 to 29 kJ/mol from ZIF-8 to IL₂₈/ZIF-8 with an increase in the IL loading. Similar improvements in Q_{st} were also observed for CH₄ with increased IL loading. Q_{st} of CH₄ increased from 13 kJ/mol in pristine ZIF-8 to 20 kJ/mol in IL₂₈/ZIF-8. The case is similar with N₂, for which it increased from approximately 8 to 13 kJ/mol upon the incorporation of IL into ZIF-8 with a loading of 28 wt%.



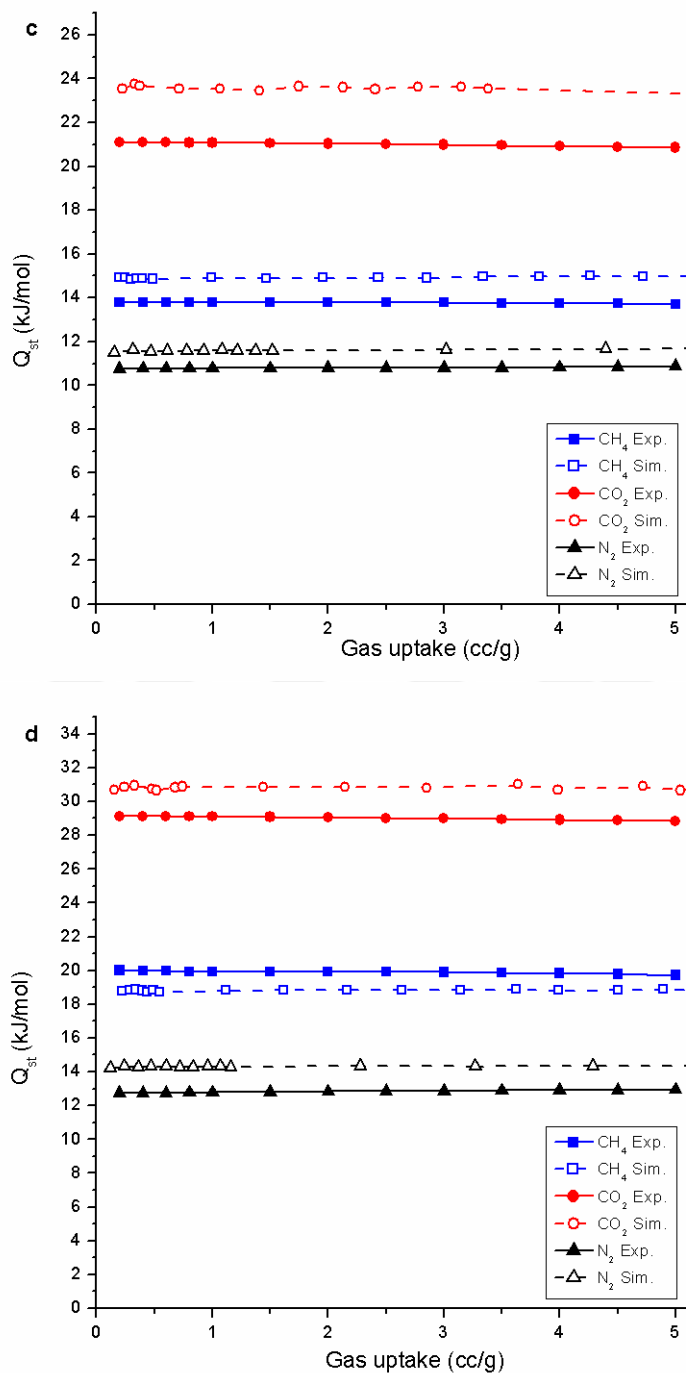


Figure 4.11: Isosteric heat of adsorption of: (a) ZIF-8, (b) IL₄/ZIF-8, (c) IL₂₀/ZIF-8, and (d) IL₂₈/ZIF-8 calculated by Equation 3.6 using the adsorption isotherms obtained at 10 and 25 °C.

Consequences of the changes in the heat of adsorption values on the gas selectivities were investigated by calculating the differences in Q_{st} values (ΔQ_{st}) of CO₂, CH₄, and N₂ for the corresponding selectivities on each sample as shown in Figure 4.12. Simulation results agreed well with the experimental results according to Figure 4.12. An increase in ΔQ_{st} of the gas pair leads to an increase in corresponding selectivities especially for CO₂/CH₄ and CO₂/N₂ at low pressures such as 0.1 bar. However, at high pressures, for example at 5 bar, the change in ΔQ_{st} does not significantly affect the gas selectivities. Thus, we infer that the interaction between MOF and IL is the dominant factor especially at low pressures influencing strongly the Q_{st} values of respective gases as we previously discussed.^[33] This is why the effect of IL on the gas selectivity becomes dominant at low pressures. However, we note that CH₄/N₂ selectivity is an exception, for which an increase in ΔQ_{st} does not lead to a significant increase in the selectivity. This behavior might suggest the presence of other factors; for instance, changes in pore volume (available space) might be a dominant factor for this gas pair.

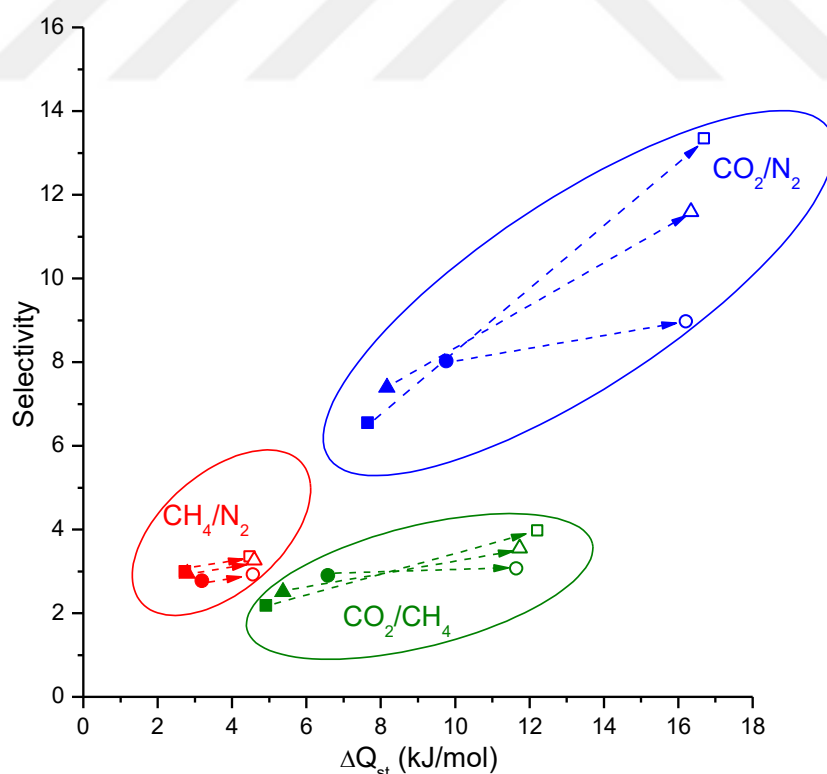


Figure 4.12: Change in the isosteric heat of adsorption of corresponding gases in ZIF-8 and IL₂₈/ZIF-8 with respect to the gas selectivities. Closed (open) symbols show selectivity of ZIF-8 (IL₂₈/ZIF-8) sample. Each symbol indicates different pressure: rectangle (■): 0.1 bar, triangle (▲): 1 bar, circle (●): 5 bar.

Chapter 5

DIFFERENT IL-MOF PAIRS

In the first part of this thesis, [BMIM][BF₄]/ZIF-8 composites with different IL loadings were investigated and the optimum IL loading was designated as 30 wt%. In the second part, other imidazolium based IL-MOF pairs ([EMIM][PF₆]/ZIF-8, [OMIM][PF₆]/ZIF-8, [C3CNMIM][NTf₂]/ZIF-8, [(EtO)2IM][NTf₂]/ZIF-8, [EMIM][SCN]/ZIF-8, [BMIM][O₂CSO₄]/ZIF-8, and [BMIM][NTf₂]/ZIF-8) with 30 wt% IL loading were characterized and performances were measured in order to compare the performances of different imidazolium-based IL incorporation. Different ILs were chosen to investigate the structural effects of ILs on gas storage and separation performances of composite materials.

5.1 Other IL-MOF Combinations

The names, anions, cations and molecular geometries of ILs chosen to examine the structural effects on performances of IL/MOF composites are given in Table 5.1. Accordingly, change in the length of alkyl group in imidazolium ring, different anions, and functional groups in imidazolium ring can be investigated.

To find out the composition of composite materials, XRF measurements were performed with the methods explained in Chapter 3. XRF results shown in Table 5.2 illustrate that ILs exist in the composite material at comparable amounts.

Table 5.1: ILs incorporated into ZIF-8.

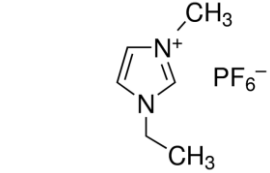
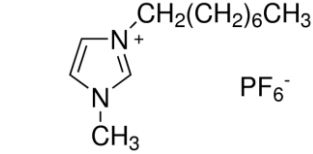
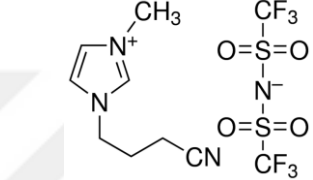
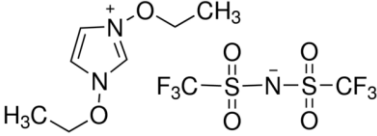
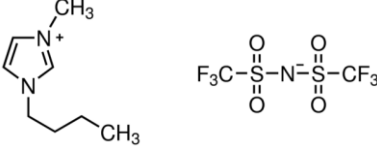
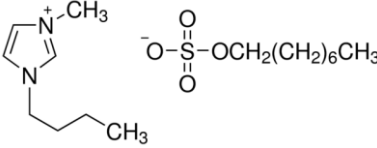
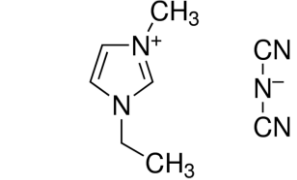
IL	Cation	Anion	Molecular Geometry
1-Ethyl-3-methylimidazolium hexafluorophosphate	[EMIM]	[PF ₆]	
1-Methyl-3-octylimidazolium hexafluorophosphate	[OMIM]	[PF ₆]	
1-(3-Cyanopropyl)-3-methylimidazolium bis(trifluoromethylsulfonyl)amide	[C ₃ CNMIM]	[NTf ₂]	
1,3-Diethoxyimidazolium bis(trifluoromethylsulfonyl)imide	[(EtO) ₂ IM]	[NTf ₂]	
1-Butyl-3-methylimidazolium bis(trifluoromethylsulfonyl)imide	[BMIM]	[NTf ₂]	
1-Butyl-3-methylimidazolium octyl sulfate	[BMIM]	[OcSO ₄]	
1-Ethyl-3-methylimidazolium dicyanamide	[EMIM]	[SCN]	

Table 5.2: XRF results of IL/MOF composites

Sample	Zn Concentration	Calculated loading (wt%)
[EMIM][PF ₆]/ZIF-8	13.35	25.3
[OMIM][PF ₆]/ZIF-8	11.94	25.5
[C ₃ CNMIM][NTf ₂]/ZIF-8	14.06	26.5
[(EtO) ₂ IM][NTf ₂]/ZIF-8	15.67	25.5
[EMIM][SCN]/ZIF-8	17.96	25.8
[BMIM][NTf ₂]/ZIF-8	13.9	24
[BMIM][OcSO ₄]/ZIF-8	16.79	24.3

SEM images given in Figure 5.1 show the morphology of the samples after incorporation of ILs. Accordingly, incorporation of [EMIM][PF₆], [OMIM][PF₆], and [BMIM][OcSO₄] incorporation did not cause any change in the morphology of ZIF-8. However, the ILs with the anion of [NTf₂] and [OcSO₄] affected the framework significantly. This effect may be originated from the excess IL loading. Since [NTf₂] and [OcSO₄] anions have relatively bigger sizes than [PF₆], excess ILs might aggregate out of the crystals. BET measurements or molecular simulations can be useful to figure out if the ILs are inside the pores of ZIF-8.

Effect of the IL incorporation on the crystal structure was analyzed with XRD patterns which were given in Figure 5.2. Remarkable shifts in the positions of the peaks were observed especially in [BMIM][OcSO₄]/ZIF-8 and [EMIM][SCN]/ZIF-8 which show the change in the interplanar distance. Also intensities changed as a result of the alteration in the electron density after incorporation. These features are the obvious signs of interactions between IL and MOF.

For the further elucidation of these interactions, we analyzed the IR bands of MOF, IL and IL/MOF samples. As seen in Figure 5.3, the peaks that belong to the pure IL appear in the spectrum of the composite material which proves the presence of IL. Additionally, shifts were observed in certain peaks in consequences of the interactions. For instance, the most obvious shifts were found in $\nu(\text{C2H})_{\text{sym}}$ vibration of the ILs which is responsible for the inter-ionic interaction. The amounts of these shifts were given in Table 5.3. As interpreted in the case of [BMIM][BF₄]/ZIF-8, electron density changes in the most of the samples which leads to the requirement of quantum-based calculations to optimize the structure of the composite before adsorption calculations.

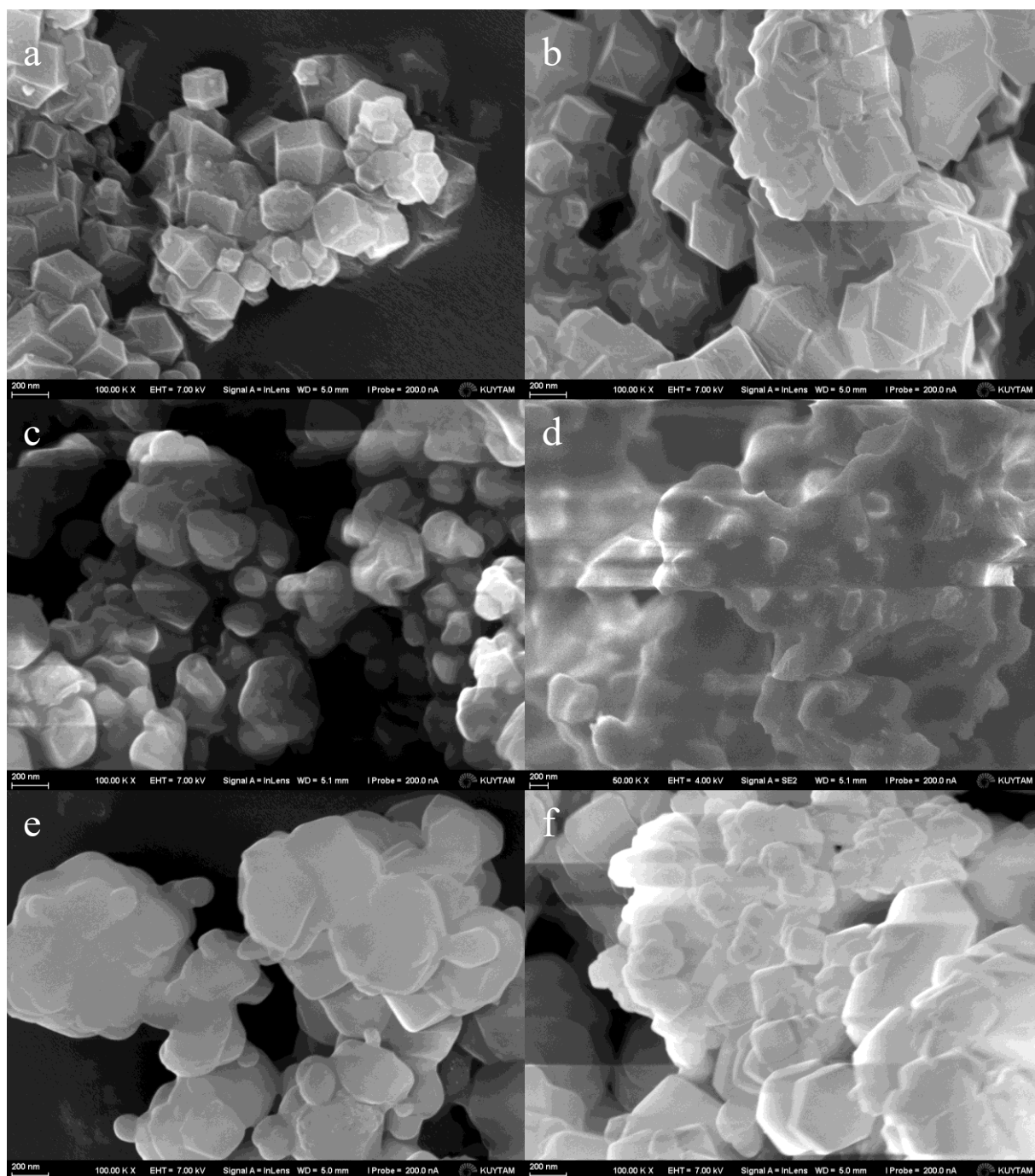


Figure 5.1: SEM images of IL/MOF composites: (a) [EMIM][PF₆]/ZIF-8, (b) [OMIM][PF₆]/ZIF-8, (c) [C₃CNMIM][NTf₂]/ZIF-8, (d) [(EtO)₂IM][NTf₂]/ZIF-8, (e) [EMIM][SCN]/ZIF-8, (f) [BMIM][OCSO₄]/ZIF-8.

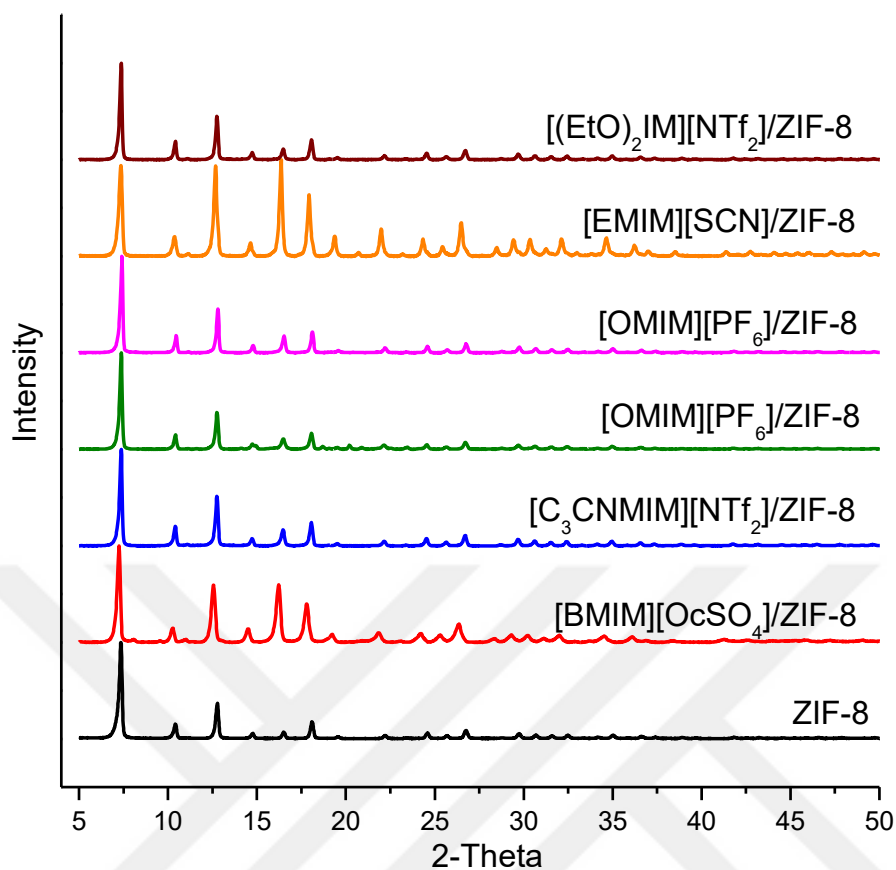
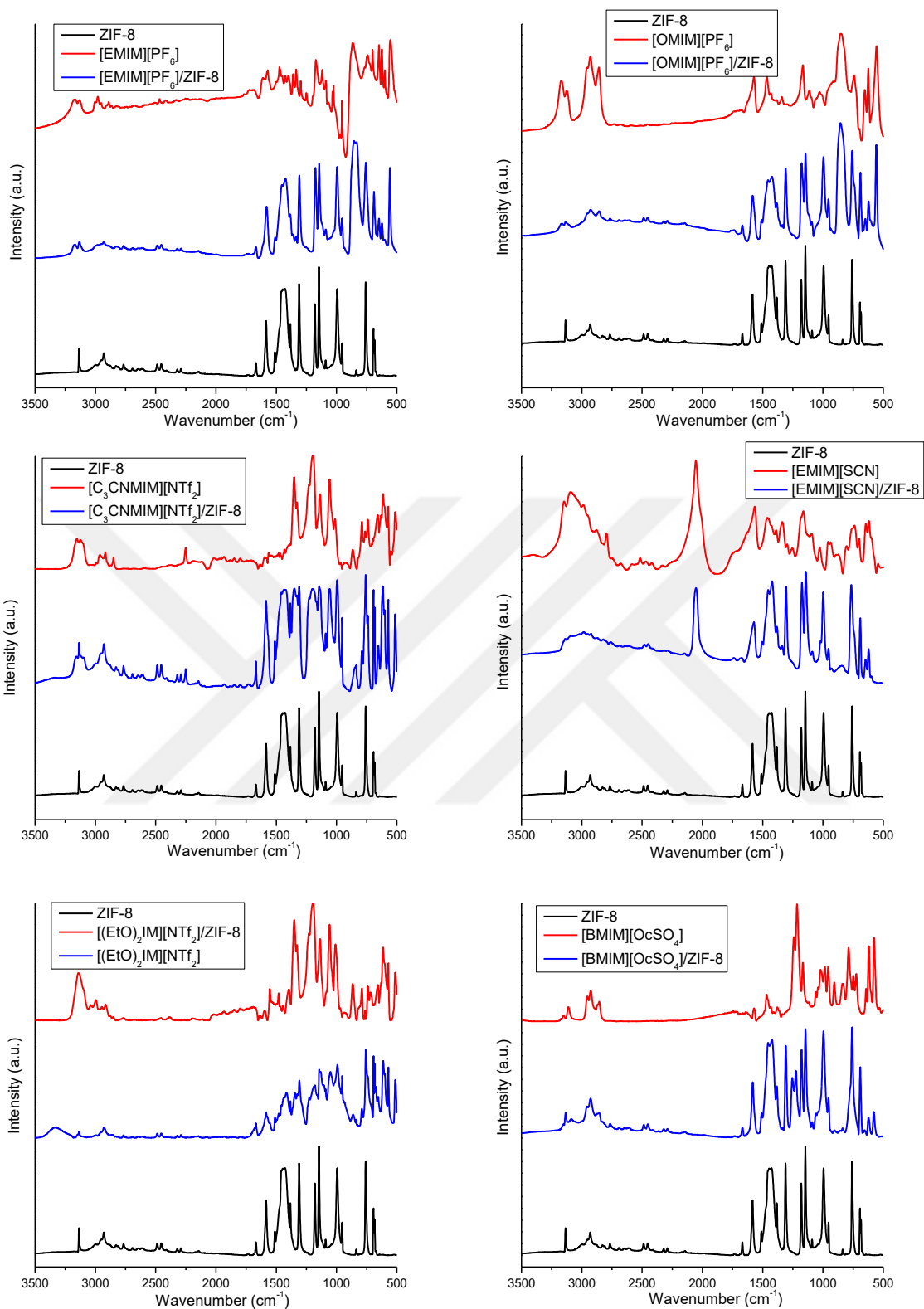


Figure 5.2: XRD pattern of ZIF-8 and IL/MOF Composites.

Gas adsorption measurements were performed with the same instrument (HPVA) at different pressures. The isotherms were obtained up to 20 bar and each gas was fitted to the Freundlich model which was given in Equation 3.4. Fit parameters were given in Table A.3. According to the isotherms given in Figure 5.4, uptakes for CO₂, CH₄ and N₂ decreased at different degrees for each composite. The highest decreases were observed in [BMIM][OcSO₄]/ZIF-8 for all gases. CO₂, CH₄ and N₂ uptakes dropped to 3.86, 1.63 and 0.63 cc STP from 14.47, 5.77 and 1.95 cc STP in [BMIM][OcSO₄]/ZIF-8 at 1 bar.



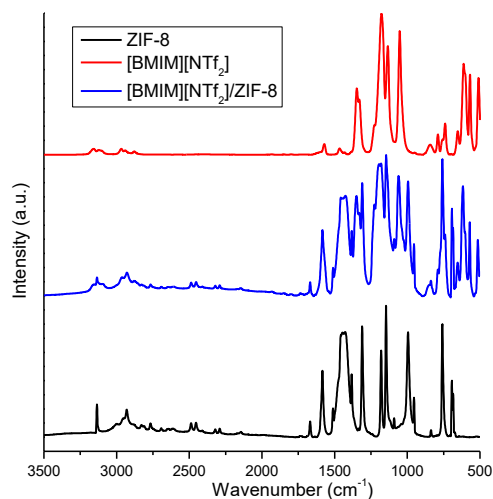
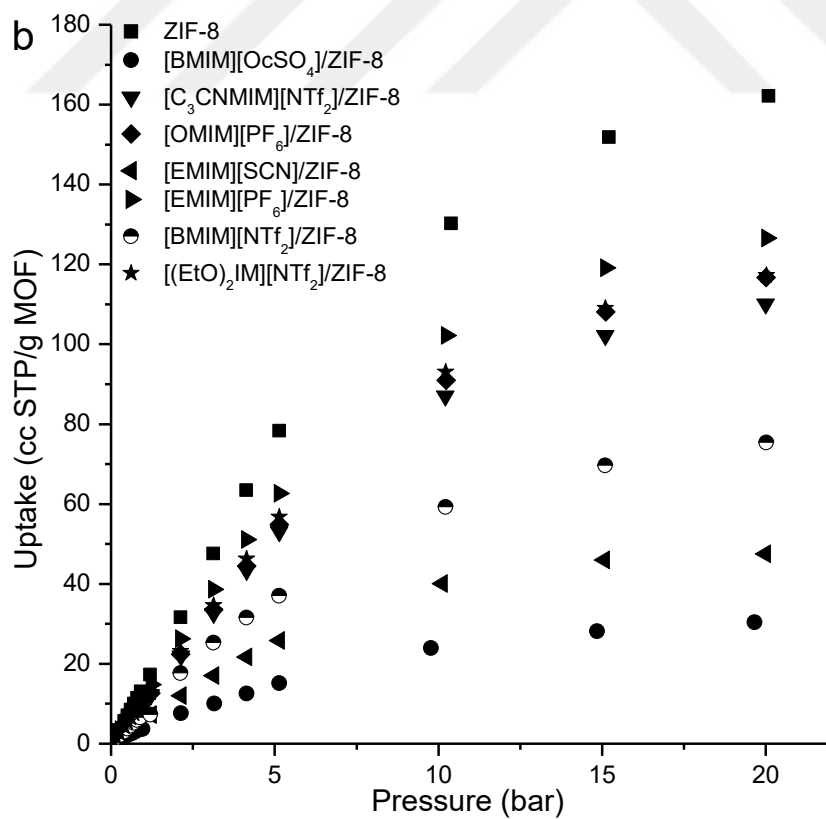
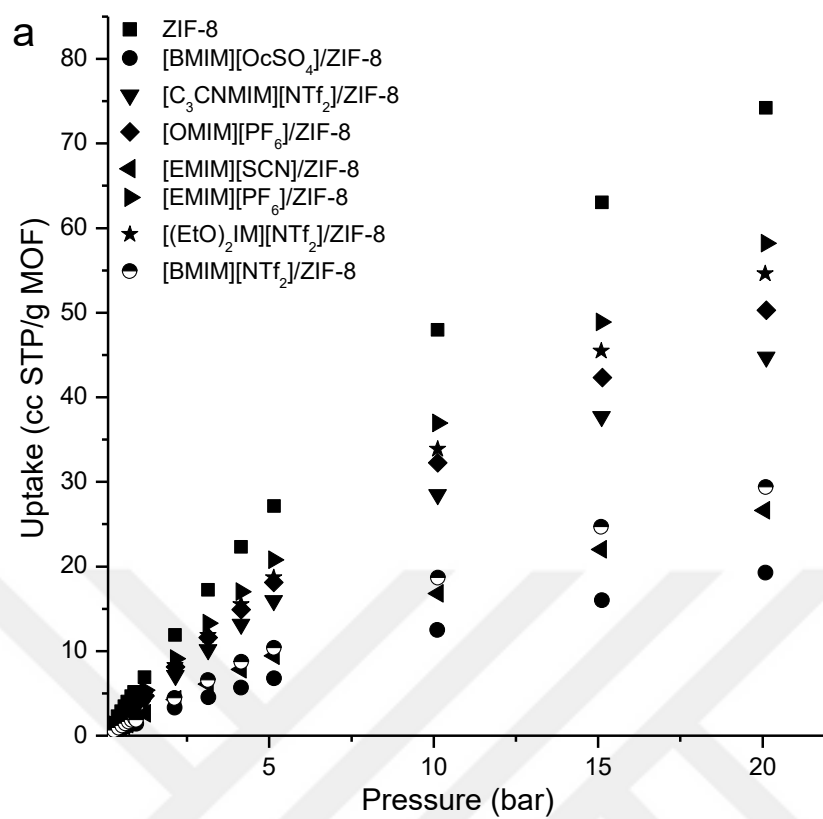


Figure 5.3: IR spectra of ZIF-8, ILs and IL/MOF composites.

Table 5.3: $\nu(\text{C2H})_{\text{sym}}$ vibration bands of pure ILs and IL/MOF composites.

IL	$\nu(\text{C2H})_{\text{sym}}$	
	Bulk	Composite
$[(\text{EtO})_2\text{IM}][\text{NTf}_2]$	3122	3130
$[\text{C}_3\text{CNMIM}][\text{NTf}_2]$	3125	3130
$[\text{EMIM}][\text{PF}_6]$	3129	3121
$[\text{EMIM}][\text{SCN}]$	3149	3152
$[\text{OMIM}][\text{PF}_6]$	3122	3122
$[\text{BMIM}][\text{OcSO}_4]$	3112	3123



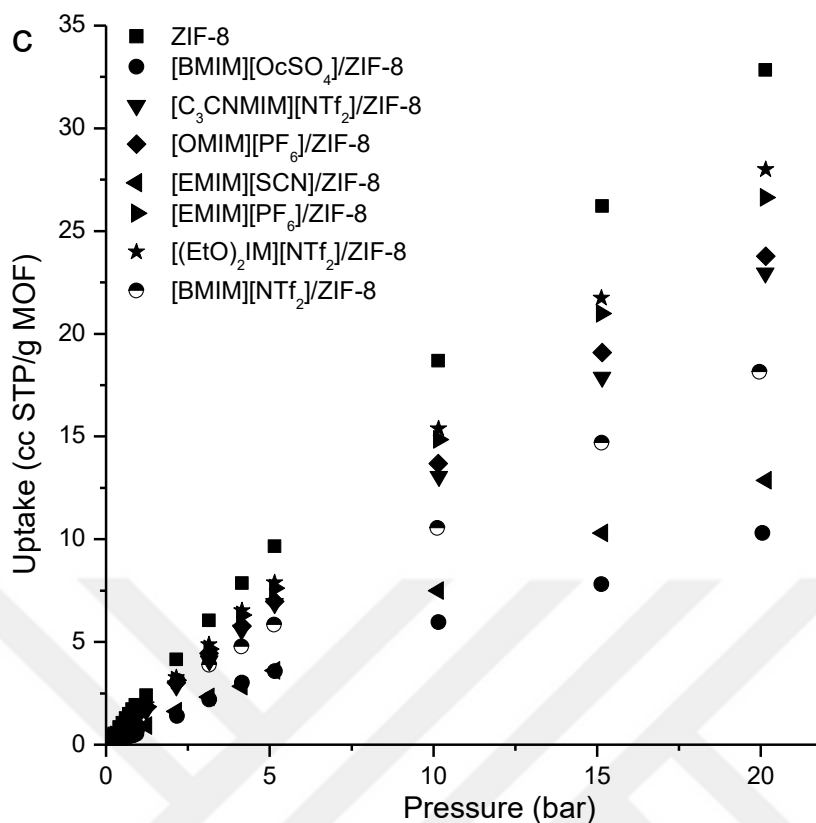
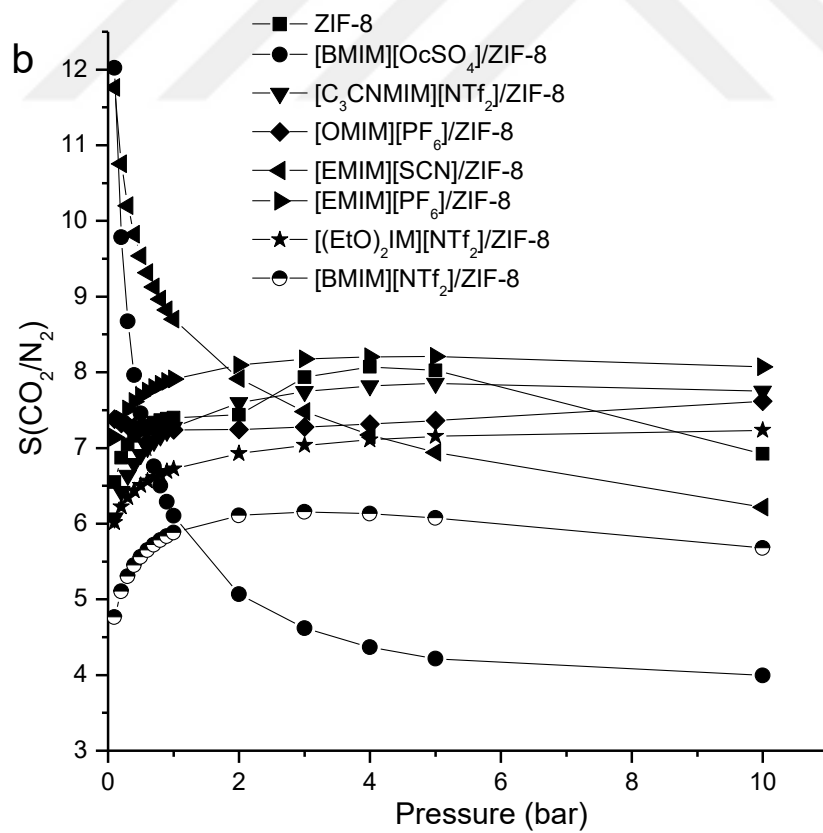
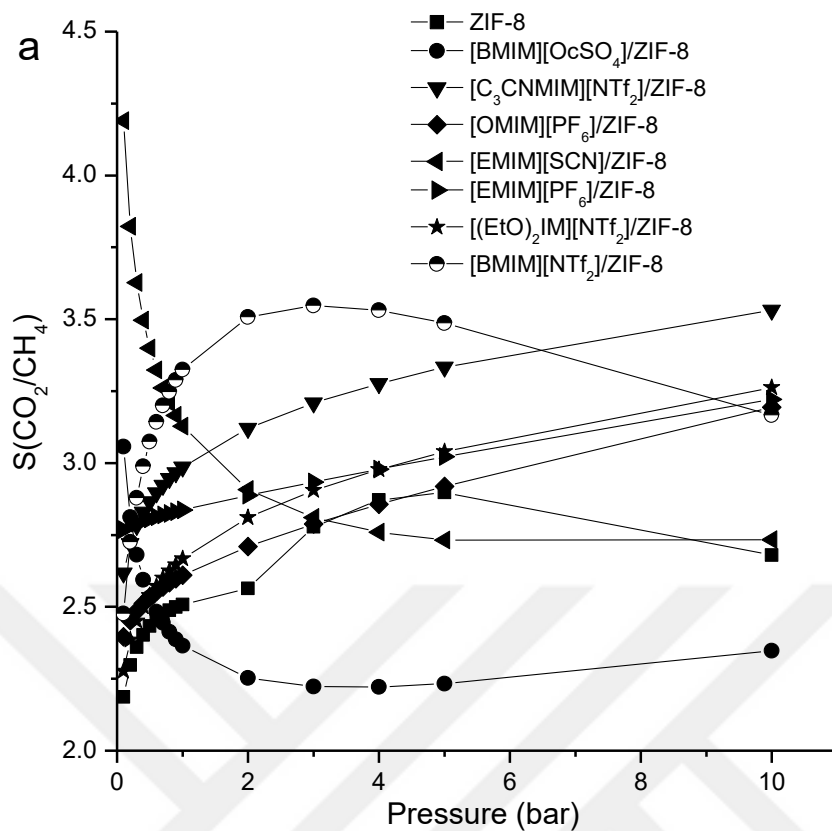


Figure 5.4: Uptake values in ZIF-8 and IL-MOF composites: (a) CH₄, (b) CO₂, (c) N₂.

The different decreases in uptakes led to change in the ideal gas selectivities. Figure 5.5 shows the ideal selectivities which were calculated by dividing the higher amount of adsorbed gas to the lower amount one. Both in CO₂/CH₄ and CO₂/N₂ selectivities, [EMIM][SCN]/ZIF-8 is dominant with remarkable selectivity values which almost doubles the selectivities of ZIF-8 at 0.1 bar. These different selectivities are originated from the distinct interactions between ILs and MOF. Keeping the amount of ILs same in each composites, it can be easily seen that the different interactions (possibly originated from the different amounts of shift in $\nu(\text{C}2\text{H})_{\text{sym}}$) leading to distinct adsorption properties. To eliminate the pore volume factor, one can also compare the performances of these composites keeping the volume same in each IL-MOF samples.



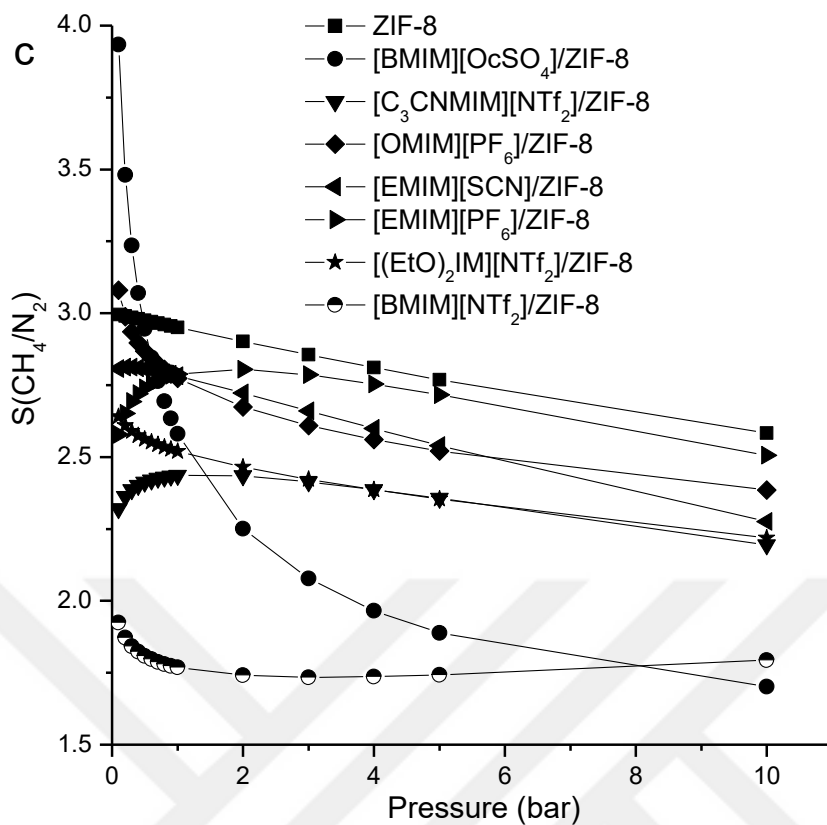


Figure 5.5: Selectivities of ZIF-8 and IL-MOF composites: (a) CO₂/CH₄ (b) CO₂/N₂ (c) CH₄/N₂.

Chapter 6

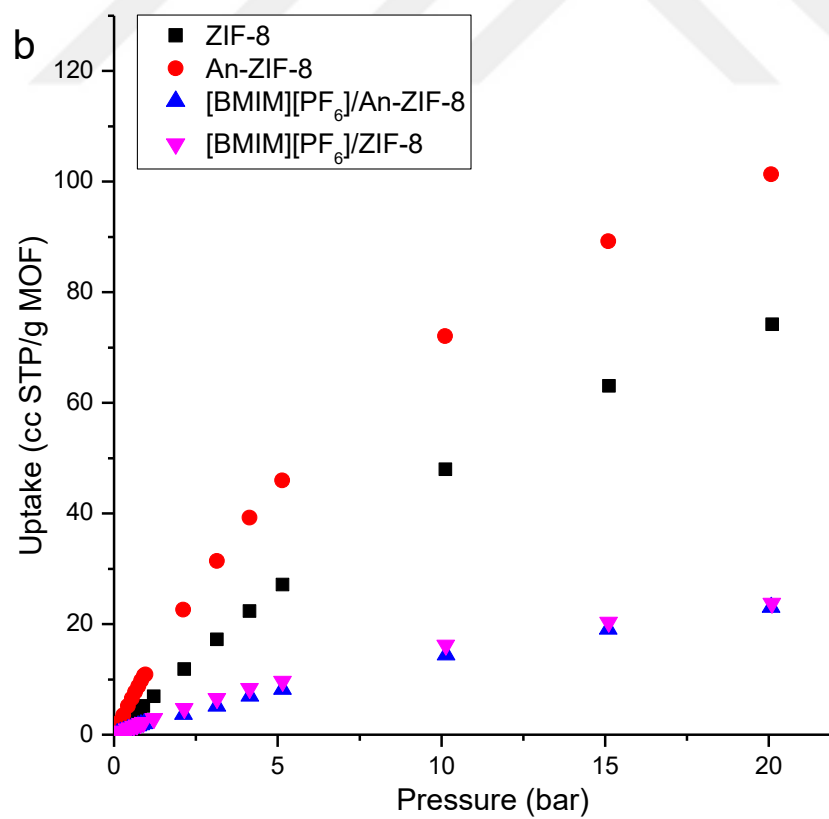
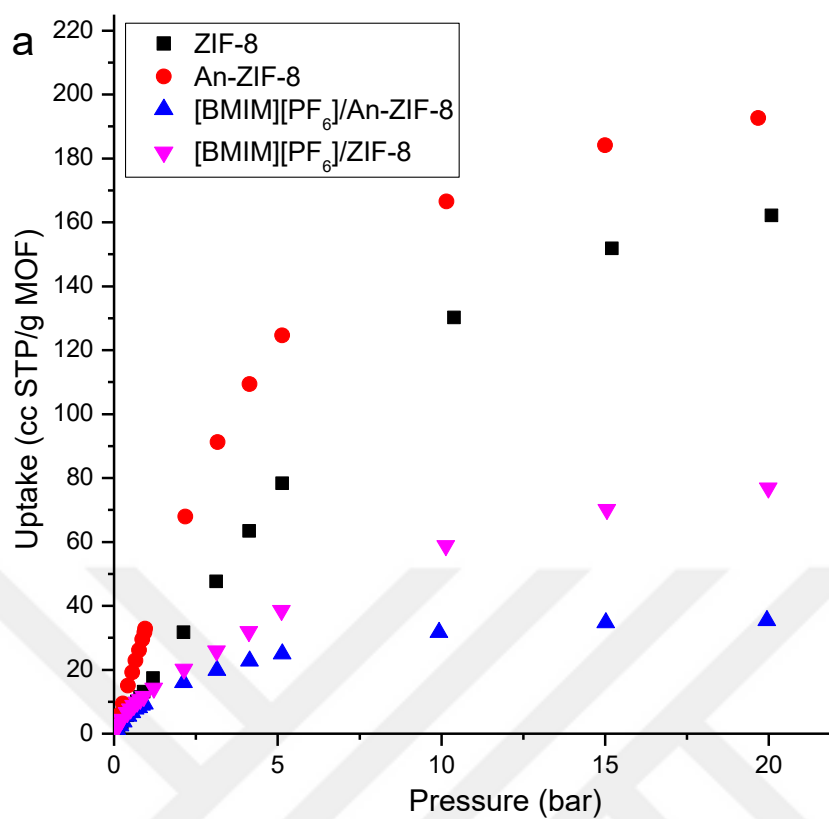
ANNEALING OF ZIF-8

One approach to modify MOF after synthesis (post-synthetic modification) is thermal treatment of the framework. This modification can be carried out without introducing any cavity occupant and it has a huge potential to reach higher gas uptake and gas separation performances.

ZIF-8 is robust and thermally stable MOF which starts to decompose above 350 °C. In order to keep the framework intact, the temperature was elevated up to the point where the isothermal treatment does not cause to the collapse of the framework. The highest temperature was found as 525 °C for 6 hours isothermal process.^[73]

The conditions where the highest CO₂ uptake was reported for the annealing process of ZIF-8 were selected to investigate CH₄, CO₂, and N₂ uptakes in annealed ZIF-8.^[73] The resulting sample was designated as An-ZIF-8. Also, we incorporated 30 wt% [BMIM][PF₆] into the pores of An-ZIF-8. For CH₄, CO₂, and N₂, static adsorption was measured with HPVA. CH₄, CO₂, and N₂ uptakes were fitted to Freundlich model and fit parameters were given in Appendix A.

As shown in Figure 5.6, the uptake values for each gas increased after annealing at 500 °C for 24 hours most likely due to the expansion in the mesopore volume of MOF resulting from the removal of the methyl group bonded to imidazolium ring in ZIF-8.^[73] At 0.1 bar, the CH₄, CO₂, and N₂ uptakes increased to 1.25, 3.17 and 0.37 cc STP from 0.58, 1.28 and 0.19 cc STP, respectively. However, in [BMIM][PF₆]/An-ZIF-8, decrease in all gases were observed. CH₄, CO₂, and N₂ uptakes dropped to 0.25, 1.64 and 0.09 cc STP at 0.1 bar as [BMIM][PF₆] occupied some of the pore volume. The decrease in CO₂ uptake is much higher as compared to that of [BMIM][PF₆]/ZIF-8^[33] samples whereas decreases in CH₄ uptake are almost same for [BMIM][PF₆]/An-ZIF-8 and [BMIM][PF₆]/ZIF-8. These differences lead to different ideal selectivities.



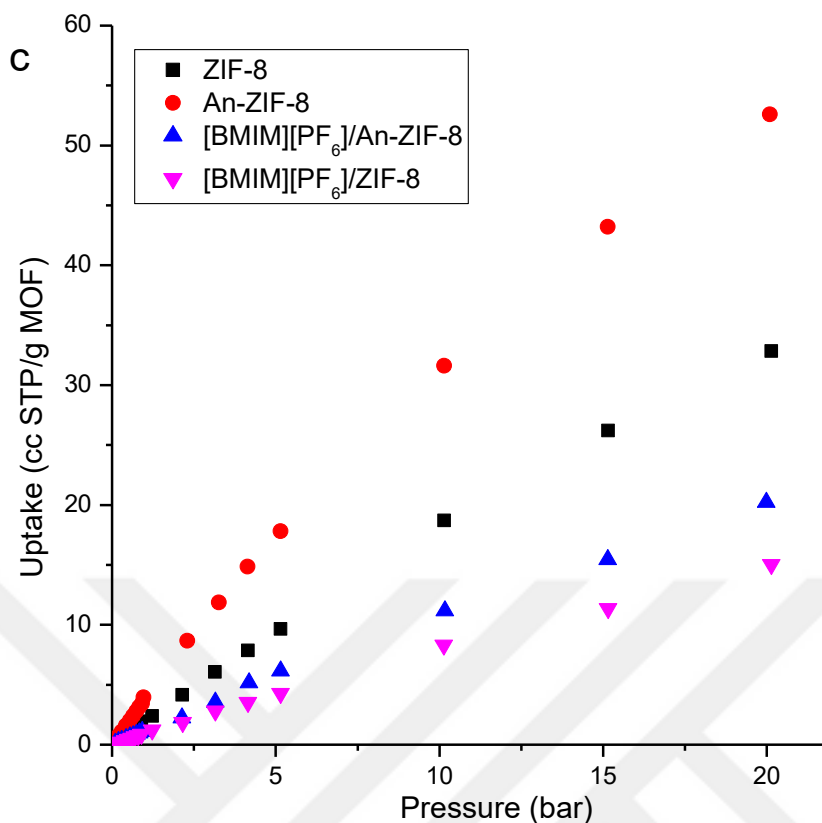
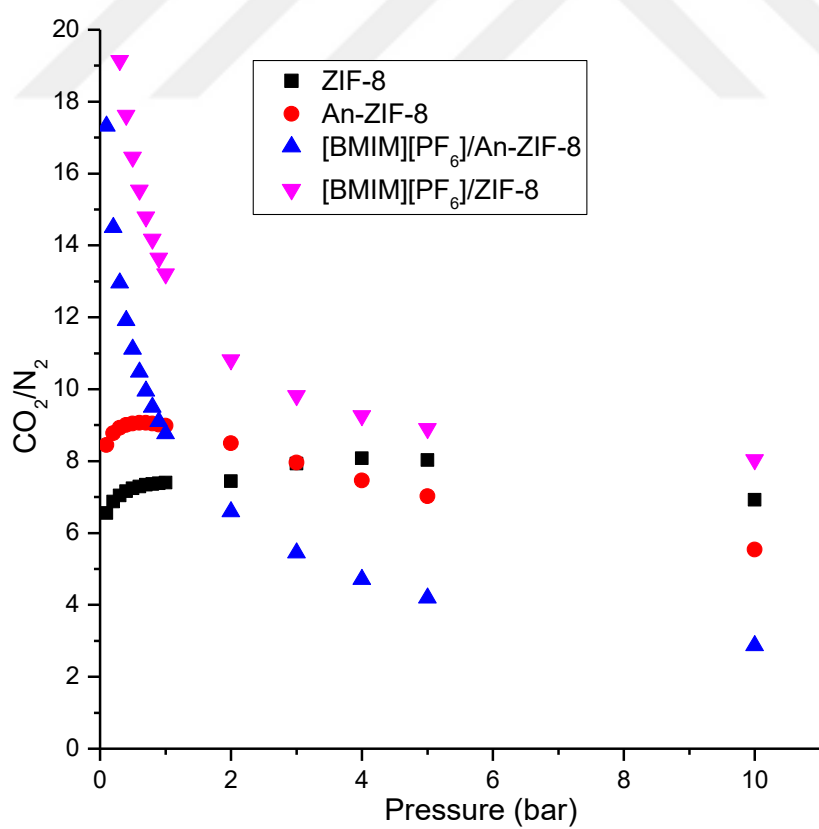
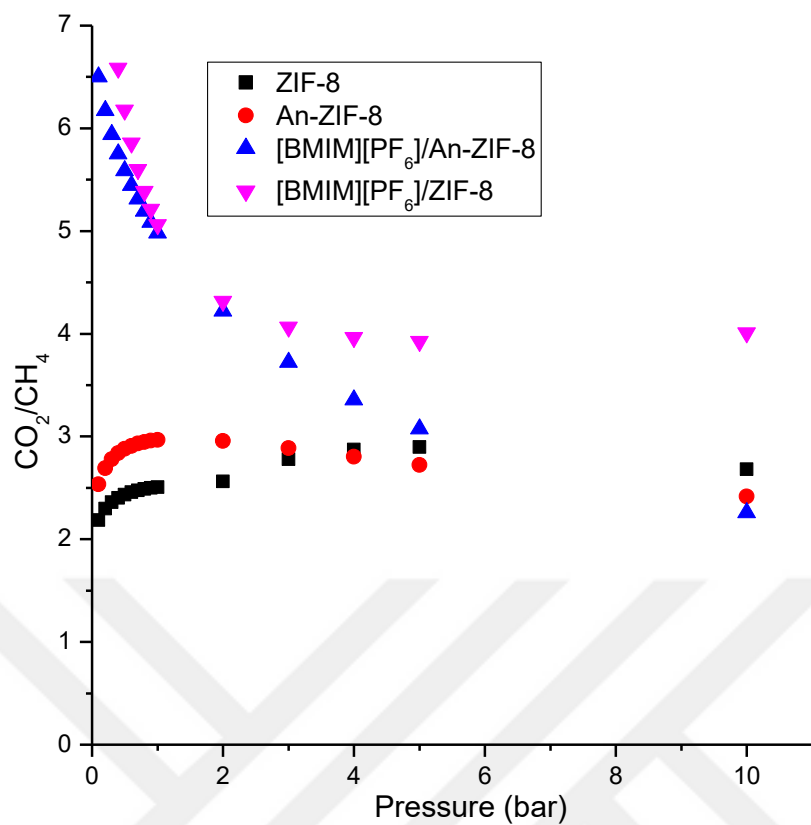


Figure 5.6: Adsorption isotherms of ZIF-8, An-ZIF-8, [BMIM][PF₆]/ZIF-8, and [BMIM][PF₆]/An-ZIF-8: (a) CO₂, (b) CH₄, (c) N₂.

As the changes in the uptake values are not identical for each gas, one can expect alteration in selectivities. Figure 5.7 shows the ideal gas selectivities in ZIF-8, An-ZIF-8 and [BMIM][PF₆]/An-ZIF-8. Accordingly, [BMIM][PF₆]/An-ZIF-8 sample outperform the CO₂/CH₄ and CO₂/N₂ selectivities of ZIF-8 up to 5 and 1 bar. At 0.1 bar, CO₂/CH₄ selectivity was calculated as 6.50 for [BMIM][PF₆]/An-ZIF-8 whereas it was calculated as 2.18 for pure ZIF-8. However, it decreased CH₄/N₂ selectivities within the entire pressure range. The improvement in the selectivities is possible due to the interactions between IL and annealed MOF. Although the differences in the selectivities of [BMIM][PF₆]/An-ZIF-8 were observed, no selectivity superior to the selectivity of [BMIM][PF₆]/ZIF-8 was obtained.



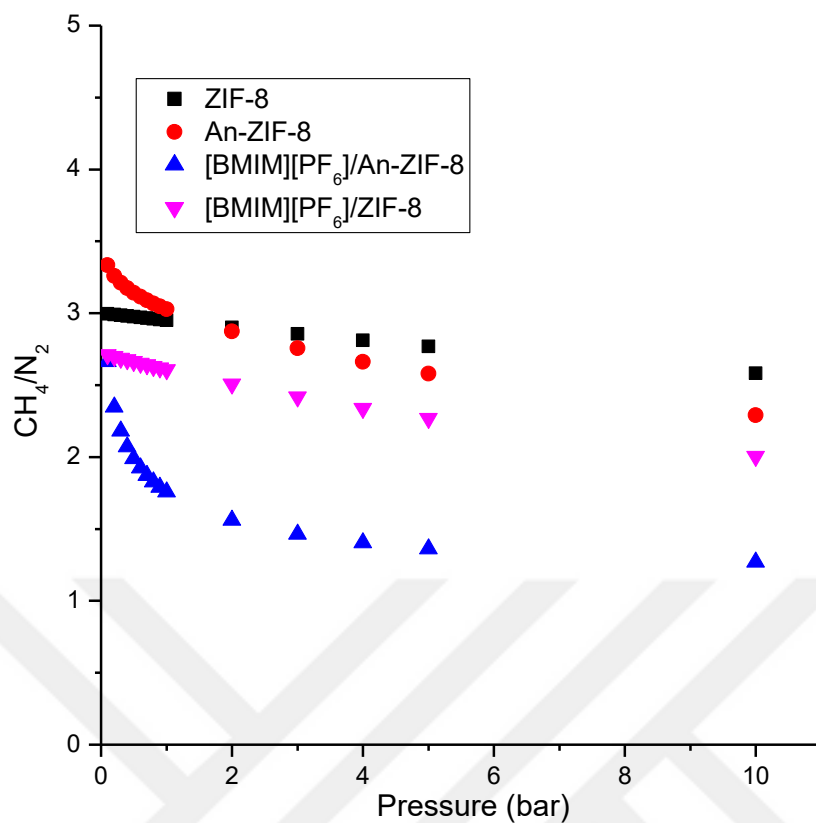


Figure 5.7: Selectivity of ZIF-8, An-ZIF-8, [BMIM][PF₆]/ZIF-8, and [BMIM][PF₆]/An-ZIF-8.

Chapter 7

CONCLUSIONS AND OUTLOOK

In this thesis, IL/MOF composites have been investigated and interactions between IL and MOFs were elucidated. The gas storage and separation performances were measured for CO₂, CH₄ and N₂ gases. Initially, [BMIM][BF₄]/ZIF-8 samples were prepared at different loadings (5, 20, and 30 wt%) and the structure of the materials were examined using different characterization techniques. Results showed that the IL was impregnated into the pores of ZIF-8 and the morphology and crystal structure remained intact after incorporation. IR results provided additional evidence on the presence of these interactions and indicated that anion of the IL was shared between the imidazolate linkers of ZIF-8 and [BMIM]⁺. As a result of these interactions, the optimum loading was found for the best gas separation performance as 30 wt%. The gas separation performance of the IL-loaded ZIF-8 was significantly modified. Results indicated that CO₂/CH₄ selectivity becomes almost twice of its value on pristine ZIF-8 at low pressures. Further analysis of the results indicated that the presence of IL modifies the gas adsorption behavior of MOF by significantly improving the heat of adsorption values. For instance Q_{st} of CO₂ increased by almost twice as much of that of N₂ does. Because this increase occurs at different extents for each gas, increase in the CO₂ being the largest, the MOF becomes more selective towards CO₂ upon the incorporation of [BMIM][BF₄].

IL/MOF concept was extended to the other pairs ([EMIM][PF₆]/ZIF-8, [OMIM][PF₆]/ZIF-8, [C3CNMIM][NTf₂]/ZIF-8, [(EtO)2IM][NTf₂]/ZIF-8, [EMIM][SCN]/ZIF-8, [BMIM][OcSO₄]/ZIF-8, and [BMIM][NTf₂]/ZIF-8) and these pairs were characterized. For most of the combinations, we observed remarkable improvements in gas separation performances due to the distinct interactions between ILs and MOF. Further examination is needed to find out the rational relationships between the structural properties of composite materials and storage-separation performances. Other than introducing IL directly into the pore of pure MOF, modification of MOF with annealing process also enables higher static capacities and slightly better selectivities. Incorporation of IL into annealed ZIF-

8 sample increases the selectivity remarkably and results showed that gas separation performances can be improved with both annealing and IL impregnation.

As a conclusion, modification of MOFs with IL incorporation and annealing provides opportunity to enhance the gas storage and separation performances. Taking the advantage of limitless number of combinations of MOFs and ILs, structure-performance relation can be examined and modeled for a desired gas separation application. To predict the sorption properties of a certain IL/MOF composite, the geometry of the initial structure can be optimized with DFT calculations and charges of the atoms can be estimated following ChelpG method and finally GCMC simulations can be performed to predict adsorption of desired gas. Also, Rietveld Refinement can be done to the crystal data of the sample prepared in the laboratory and obtained a unit cell which can be used in prediction of the adsorption of a number of gases.

BIBLIOGRAPHY

- [1] J. A. Mason, M. Veenstra, J. R. Long, *Chemical Science* **2014**, *5*, 32-51.
- [2] D. W. Keith, *Science* **2009**, *325*, 1654-1655.
- [3] F. Karadas, M. Atilhan, S. Aparicio, *Energy & Fuels* **2010**, *24*, 5817-5828.
- [4] K. M. K. Yu, I. Curcic, J. Gabriel, S. C. E. Tsang, *ChemSusChem* **2008**, *1*, 893-899.
- [5] J. Rouquerol, F. Rouquerol, P. Llewellyn, G. Maurin, K. S. Sing, *Adsorption by Powders and Porous Solids: Principles, Methodology and Applications*, Academic press, **2013**.
- [6] R. E. Morris, P. S. Wheatley, *Angewandte Chemie International Edition* **2008**, *47*, 4966-4981.
- [7] H.-C. Zhou, J. R. Long, O. M. Yaghi, *Chemical Reviews* **2012**, *112*, 673-674.
- [8] J. R. Long, O. M. Yaghi, *Chemical Society Reviews* **2009**, *38*, 1213-1214.
- [9] O. K. Farha, I. Eryazici, N. C. Jeong, B. G. Hauser, C. E. Wilmer, A. A. Sarjeant, R. Q. Snurr, S. T. Nguyen, A. Özgür. Yazaydın, J. T. Hupp, *Journal of the American Chemical Society* **2012**, *134*, 15016-15021.
- [10] J.-R. Li, R. J. Kuppler, H.-C. Zhou, *Chemical Society Reviews* **2009**, *38*, 1477-1504.
- [11] N. Stock, S. Biswas, *Chemical Reviews* **2011**, *112*, 933-969.
- [12] Z. Wang, S. M. Cohen, *Chemical Society Reviews* **2009**, *38*, 1315-1329.
- [13] N. V. Plechkova, K. R. Seddon, *Chemical Society Reviews* **2008**, *37*, 123-150.
- [14] R. D. Rogers, K. R. Seddon, *Science* **2003**, *302*, 792-793.
- [15] H. Tokuda, S. Tsuzuki, M. A. B. H. Susan, K. Hayamizu, M. Watanabe, *The Journal of Physical Chemistry B* **2006**, *110*, 19593-19600.
- [16] P. Wasserscheid, T. Welton, *Ionic Liquids in Synthesis*, John Wiley & Sons, **2008**.
- [17] S. Pandey, *Analytica Chimica Acta* **2006**, *556*, 38-45.
- [18] M. Babucci, A. Uzun, *Journal of Molecular Liquids* **2016**, *216*, 293-297.
- [19] C. Casado-Coterillo, A. Fernández-Barquín, B. Zornoza, C. Téllez, J. Coronas, Á. Irabien, *RSC Advances* **2015**, *5*, 102350-102361.
- [20] L. Hao, P. Li, T. Yang, T.-S. Chung, *Journal of Membrane Science* **2013**, *436*, 221-231.
- [21] H. Li, L. Tuo, K. Yang, H.-K. Jeong, Y. Dai, G. He, W. Zhao, *Journal of Membrane Science* **2016**, *511*, 130-142.
- [22] J. Ma, Y. Ying, X. Guo, H. Huang, D. Liu, C. Zhong, *Journal of Materials Chemistry A* **2016**, *4*, 7281-7288.

- [23] R. Lin, L. Ge, H. Diao, V. Rudolph, Z. Zhu, *ACS Applied Materials & Interfaces* **2016**, *8*, 32041-32049.
- [24] Z. Li, Y. Xiao, W. Xue, Q. Yang, C. Zhong, *The Journal of Physical Chemistry C* **2015**, *119*, 3674-3683.
- [25] Y. Ban, Z. Li, Y. Li, Y. Peng, H. Jin, W. Jiao, A. Guo, P. Wang, Q. Yang, C. Zhong, *Angewandte Chemie* **2015**, *127*, 15703-15707.
- [26] F. Da Silva, G. Magalhães, E. Jardim, J. Silvestre-Albero, A. Sepúlveda-Escribano, D. de Azevedo, S. de Lucena, *Adsorption Science & Technology* **2015**, *33*, 223-242.
- [27] N. R. Dhumal, M. P. Singh, J. A. Anderson, J. Kiefer, H. J. Kim, *The Journal of Physical Chemistry C* **2016**, *120*, 3295-3304.
- [28] Y. Chen, Z. Hu, K. M. Gupta, J. Jiang, *The Journal of Physical Chemistry C* **2011**, *115*, 21736-21742.
- [29] K. M. Gupta, Y. Chen, Z. Hu, J. Jiang, *Physica Chemistry Chemical Physics* **2012**, *14*, 5785-5794.
- [30] J. M. Vicent-Luna, J. J. Gutiérrez-Sevillano, J. A. Anta, S. Calero, *The Journal of Physical Chemistry C* **2013**, *117*, 20762-20768.
- [31] W. Xue, Z. Li, H. Huang, Q. Yang, D. Liu, Q. Xu, C. Zhong, *Chemical Engineering Science* **2016**, *140*, 1-9.
- [32] K. B. Sezginel, S. Keskin, A. Uzun, *Langmuir* **2016**, *32*, 1139-1147.
- [33] F. P. Kinik, C. Altintas, V. Balci, B. Koyuturk, A. Uzun, S. Keskin, *ACS Applied Materials & Interfaces* **2016**.
- [34] H. Li, M. Eddaoudi, M. O'Keeffe, O. M. Yaghi, *Nature* **1999**, *402*, 276-279.
- [35] L. Vidal, M.-L. Riekkola, A. Canals, *Analytica Chimica Acta* **2012**, *715*, 19-41.
- [36] P. Kinik, A. Uzun, S. Keskin, *ChemSusChem*.
- [37] R. E. Morris, *Chemical Communications* **2009**, 2990-2998.
- [38] L. Xu, B. Liu, S.-X. Liu, H. Jiao, B. de Castro, L. Cunha-Silva, *CrystEngComm* **2014**, *16*, 10649-10657.
- [39] N. A. Khan, Z. Hasan, S. H. Jung, *Chemistry - A European Journal* **2014**, *20*, 376-380.
- [40] Q.-X. Luo, X.-D. Song, M. Ji, S.-E. Park, C. Hao, Y.-Q. Li, *Applied Catalysis A* **2014**, *478*, 81-90.
- [41] Q.-X. Luo, B.-W. An, M. Ji, S.-E. Park, C. Hao, Y.-Q. Li, *Journal of Porous Materials* **2015**, *22*, 247-259.
- [42] C. Chen, Z. Wu, Y. Que, B. Li, Q. Guo, Z. Li, L. Wang, H. Wan, G. Guan, *RSC Advances* **2016**, *6*, 54119-54128.

- [43] H. Wan, C. Chen, Z. Wu, Y. Que, Y. Feng, W. Wang, L. Wang, G. Guan, X. Liu, *ChemCatChem* **2015**, *7*, 441-449.
- [44] M. Han, Z. Gu, C. Chen, Z. Wu, Y. Que, Q. Wang, H. Wan, G. Guan, *RSC Advances* **2016**, *6*, 37110-37117.
- [45] A. Nasrollahpour, S. Moradi, *Microporous and Mesoporous Materials* **2017**, *243*, 47-55.
- [46] B. Koyuturk, C. Altintas, F. P. Kinik, S. Keskin, A. Uzun, *The Journal of Physical Chemistry C* **2017**, *121*, 10370-10381.
- [47] A. Nasrollahpour, S. Moradi, M. Baniamerian, *Food Analytical Methods* **2017**, 1-12.
- [48] S. Abednatanzi, A. Abbasi, M. Masteri-Farahani, *Catalysis Communications* **2017**, *96*, 6-10.
- [49] S. Abednatanzi, K. Leus, P. G. Derakhshandeh, F. Nahra, K. De Keukeleere, K. Van Hecke, I. Van Driessche, A. Abbasi, S. P. Nolan, P. Van Der Voort, *Catalysis Science & Technology* **2017**.
- [50] H. M. Hassan, M. A. Betiha, S. K. Mohamed, E. El-Sharkawy, E. A. Ahmed, *Journal of Molecular Liquids* **2017**.
- [51] J. Wu, Y. Gao, W. Zhang, Y. Tan, A. Tang, Y. Men, B. Tang, *Applied Organometallic Chemistry* **2015**, *29*, 96-100.
- [52] K. Fujie, T. Yamada, R. Ikeda, H. Kitagawa, *Angewandte Chemie International Edition* **2014**, *53*, 11302-11305.
- [53] K. Fujie, R. Ikeda, K. Otsubo, T. Yamada, H. Kitagawa, *Chemistry of Materials* **2015**, *27*, 7355-7361.
- [54] K. Fujie, K. Otsubo, R. Ikeda, T. Yamada, H. Kitagawa, *Chemical Science* **2015**, *6*, 4306-4310.
- [55] X. L. Sun, W. H. Deng, H. Chen, H. L. Han, J. M. Taylor, C. Q. Wan, G. Xu, *Chemistry - A European Journal* **2016**.
- [56] Y. Xin, C. Wang, Y. Wang, J. Sun, Y. Gao, *RSC Advances* **2017**, *7*, 1697-1700.
- [57] I. Ahmed, T. Panja, N. A. Khan, M. Sarker, J.-S. Yu, S. H. Jung, *ACS Applied Materials & Interfaces* **2017**.
- [58] N. A. Khan, Z. Hasan, S. H. Jung, *Chemical Communications* **2016**, *52*, 2561-2564.
- [59] Q.-X. Luo, M. Ji, M.-h. Lu, C. Hao, J.-S. Qiu, Y.-Q. Li, *Journal of Materials Chemistry A* **2013**, *1*, 6530-6534.
- [60] Z. Li, W. Wang, Y. Chen, C. Xiong, G. He, Y. Cao, H. Wu, M. D. Guiver, Z. Jiang, *Journal of Materials Chemistry A* **2016**, *4*, 2340-2348.

- [61] J. Lee, O. K. Farha, J. Roberts, K. A. Scheidt, S. T. Nguyen, J. T. Hupp, *Chemical Society Reviews* **2009**, *38*, 1450-1459.
- [62] X. Kang, J. Zhang, W. Shang, T. Wu, P. Zhang, B. Han, Z. Wu, G. Mo, X. Xing, *Journal of the American Chemical Society* **2014**, *136*, 3768-3771.
- [63] J. Tharun, K.-M. Bhin, R. Roshan, D. W. Kim, A. C. Kathalikkattil, R. Babu, H. Y. Ahn, Y. S. Won, D.-W. Park, *Green Chemistry* **2016**, *18*, 2479-2487.
- [64] D. Julião, A. C. Gomes, M. Pillinger, L. Cunha-Silva, B. de Castro, I. S. Gonçalves, S. S. Balula, *Fuel Processing Technology* **2015**, *131*, 78-86.
- [65] L. Peng, J. Zhang, S. Yang, B. Han, X. Sang, C. Liu, G. Yang, *Green Chemistry* **2015**, *17*, 4178-4182.
- [66] L.-G. Ding, B.-J. Yao, W.-L. Jiang, J.-T. Li, Q.-J. Fu, Y.-A. Li, Z.-H. Liu, J.-P. Ma, Y.-B. Dong, *Inorganic Chemistry* **2017**, *56*, 2337-2344.
- [67] G. Dong, H. Li, V. Chen, *Journal of Materials Chemistry A* **2013**, *1*, 4610-4630.
- [68] L. M. Robeson, *Journal of Membrane Science* **1991**, *62*, 165-185.
- [69] L. M. Robeson, *Journal of Membrane Science* **2008**, *320*, 390-400.
- [70] S. Brunauer, P. H. Emmett, E. Teller, *Journal of the American Chemical Society* **1938**, *60*, 309-319.
- [71] M. Wojdyr, *Journal of Applied Crystallography* **2010**, *43*, 1126-1128.
- [72] S. R. Venna, M. A. Carreon, *Journal of the American Chemical Society* **2009**, *132*, 76-78.
- [73] S. Gadipelli, W. Travis, W. Zhou, Z. Guo, *Energy & Environmental Science* **2014**, *7*, 2232-2238.
- [74] M. Babucci, A. Akçay, V. Balci, A. Uzun, *Langmuir* **2015**, *31*, 9163-9176.
- [75] A. Akçay, V. Balci, A. Uzun, *Thermochimica Acta* **2014**, *589*, 131-136.
- [76] M. Babucci, V. Balci, A. Akçay, A. Uzun, *The Journal of Physical Chemistry C* **2016**, *120*, 20089-20102.
- [77] H. P. Steinrück, J. Libuda, P. Wasserscheid, T. Cremer, C. Kolbeck, M. Laurin, F. Maier, M. Sobota, P. Schulz, M. Stark, *Advanced Materials* **2011**, *23*, 2571-2587.
- [78] J. Pérez-Pellitero, H. Amrouche, F. R. Siperstein, G. Pirngruber, C. Nieto-Draghi, G. Chaplais, A. Simon-Masseron, D. Bazer-Bachi, D. Peralta, N. Bats, *Chemistry - A European Journal* **2010**, *16*, 1560-1571.

APPENDIX A: Supplementary Information for Fit Parameters

Table A.1: Fit parameters for CO₂, CH₄ and N₂ measured at different temperatures for ZIF-8.

Fit Parameters	ZIF-8			IL ₄ /ZIF-8		
	CH ₄	CO ₂	N ₂	CH ₄	CO ₂	N ₂
a₀	-1543.95	-2204.94	-972.16	-1727.12	-2204.94	-1171.98
a₁	0.58	-5.31	-1.40	0.51	-5.31	-3.14
a₂	-0.12	0.65	0.92	-0.13	0.65	0.18
a₃	-0.13	-0.02	-0.02	-0.11	-0.02	0.00
a₄	0.01	0.00	0.00	0.01	0.00	0.00
a₅	0.00	0.00	0.00	0.00	0.00	0.00
b₀	10.36	10.69	8.84	11.05	10.69	9.65
b₁	-0.01	0.00	0.00	-0.01	0.00	-0.01
b₂	0.00	0.00	0.00	0.00	0.00	0.00

Fit Parameters	IL ₂₀ /ZIF-8			IL ₂₈ /ZIF-8		
	CH ₄	CO ₂	N ₂	CH ₄	CO ₂	N ₂
a₀	-1658.31	-2537.63	-1295.54	-2411.28	-3503.71	-1531.05
a₁	1.01	0.73	-1.10	35.30	0.78	-5.78
a₂	1.05	0.33	0.23	-27.08	0.45	0.28
a₃	-1.19	-0.01	-0.13	8.81	-0.02	0.00
a₄	0.38	0.00	0.03	-1.00	0.00	0.00
a₅	-0.02	0.00	0.00	0.03	0.00	0.00
b₀	11.02	11.77	10.40	13.92	15.23	11.44
b₁	0.06	0.00	0.03	0.01	0.00	0.05
b₂	-0.02	0.00	0.00	-0.01	0.00	-0.01

Table A.2: Parameters of dual site Langmuir and Freundlich fits.

	ZIF-8				IL ₄ /ZIF-8				IL ₂₀ /ZIF-8				IL ₂₈ /ZIF-8			
	CO ₂ ^a	CO ₂ ^b	CH ₄	N ₂	CO ₂ ^a	CO ₂ ^b	CH ₄	N ₂	CO ₂ ^a	CO ₂ ^b	CH ₄	N ₂	CO ₂	CH ₄	N ₂	
A	220.00	220.00	120.94	185.62	250.00	203.50	105.76	85.21	110.00	162.82	89.56	49.98	147.48	2.08	42.71	
B	14.20	17.10	40.92	141.34	16.65	15.62	37.40	75.17	7.76	13.69	26.75	50.00	12.93	24.01	100.00	
C	1.08	1.37	120.95	91.54	1.07	1.34	105.76	68.63	1.00	1.18	57.89	31.66	0.96	72.91	49.51	
D			40.92	139.42			37.40	97.80			53.87	50.00		24.16	100.00	

^a Freundlich fit parameters between 0.1-1 bar. ^b Freundlich fit parameters between 1-10 bar

$$n = \frac{PA}{P+B} + \frac{PC}{P+D} \quad (1)$$

$$n = \frac{AP^c}{B + P^c} \quad (2)$$

n is uptake amount (cm³), P is pressure (bar).

Table A.3: Fit parameters for IL/MOF composites

	[OMIM][PF ₆]/ZIF-8			[EMIM][SCN]/ZIF-8			[EMIM][PF ₆]/ZIF-8			[C ₃ CNMIM][NTf ₂]/ZIF-8		
	CH ₄	CO ₂	N ₂	CH ₄	CO ₂	N ₂	CH ₄	CO ₂	N ₂	CH ₄	CO ₂	N ₂
A	172.584	1721.54	100	73.4947	753.339	500	174.007	1185.37	5055.58	150.519	688.279	897.998
B	41.9669	163.22	68.058	35.7815	119.543	695.202	39.0872	95.2851	3247.52	43.4032	67.0037	644.266
C	0.99779	1.02812	1.03977	1.01951	0.8849	1.01317	1.01764	1.02235	0.9737	1.00037	1.05452	0.971
	[(EtO) ₂ IM][NTf ₂]/ZIF-8			[BMIM][OcSO ₄]/ZIF-8			[BMIM][NTf ₂]/ZIF-8					
	CH ₄	CO ₂	N ₂	CH ₄	CO ₂	N ₂	CH ₄	CO ₂	N ₂			
A	267.682	1500.94	511	20	73.1493	12.4618	100.607	128.125	37.399			
B	65.2446	138.272	317.689	11.2284	17.9143	18.6628	45.5981	16.8511	29.6337			
C	0.97028	1.03594	0.9859	1.05689	0.93248	1.22758	1.01619	1.15871	1.05749			

Table A.4: Fit parameters for Annealed ZIF-8 and [BMIM][PF₆]/Annealed ZIF-8

	Annealed ZIF-8			[BMIM][PF ₆]/Annealed ZIF-8		
	CH ₄	CO ₂	N ₂	CH ₄	CO ₂	N ₂
A	176.9142	271.6198	135.0226	97.89971	48.3194	50.03405
B	14.36256	6.947551	34.50424	47.97282	3.85074	43.00405
C	0.989303	1.085142	1.01628	0.905368	0.867255	1.087303

APPENDIX B: Surface Area/Pore Volume-Loading Correlations

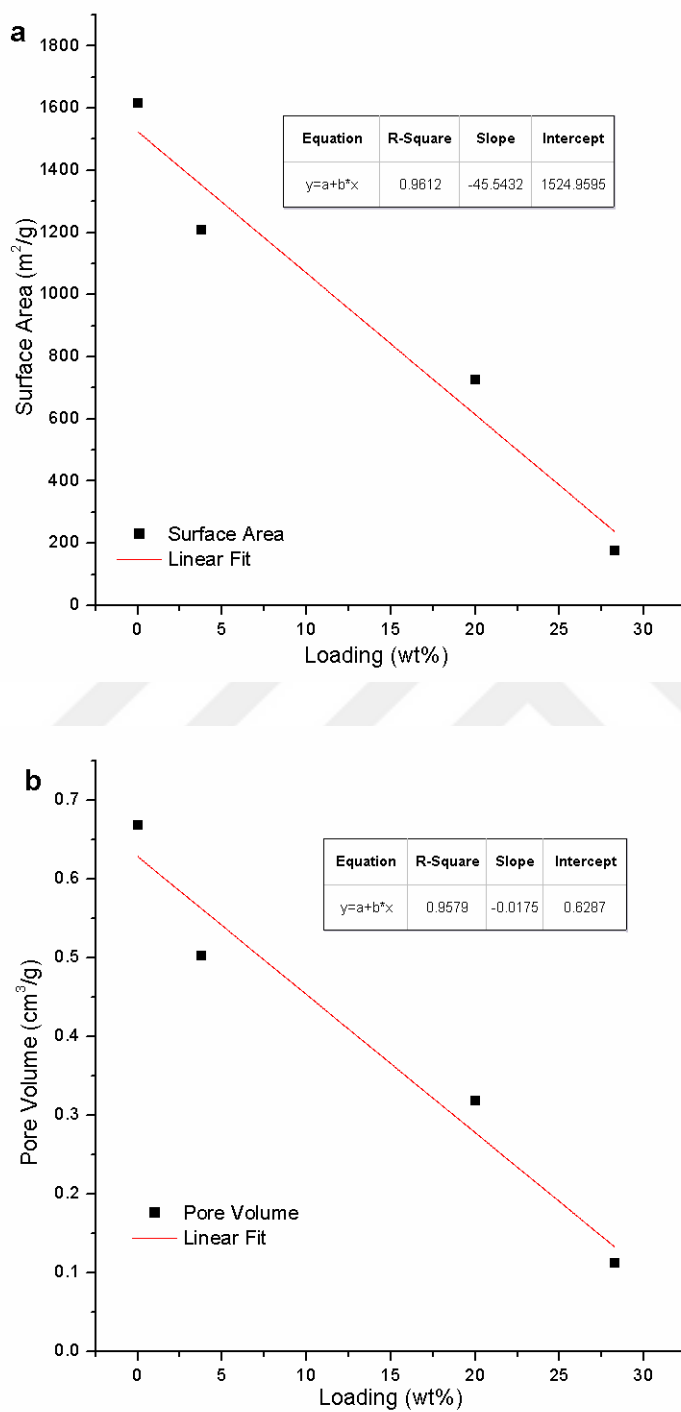


Figure B.1: Linear correlations: (a) IL loading-surface area (b) IL loading-pore volume.

APPENDIX C: Supplementary Information for IR Deconvolution

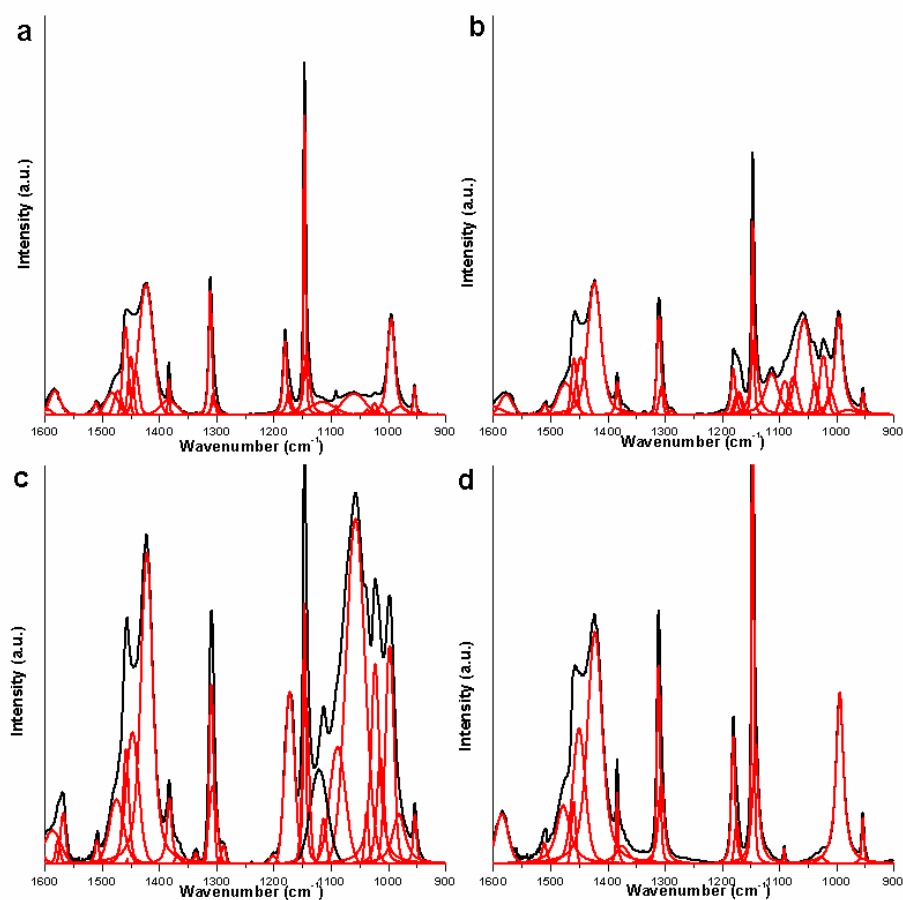


Figure C.1: Deconvoluted IR peaks between 900-1600 cm⁻¹ (a) IL₄/ZIF-8, (b) IL₂₀/ZIF-8, (c) IL₂₈/ZIF-8 (d) ZIF-8.

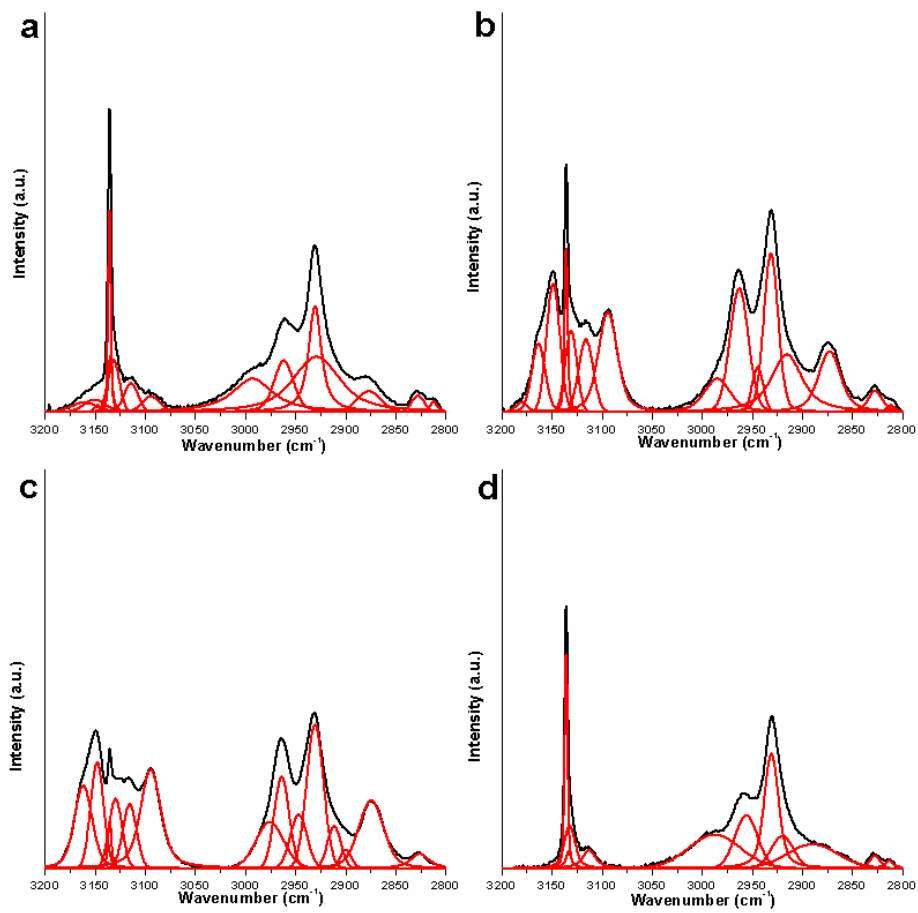
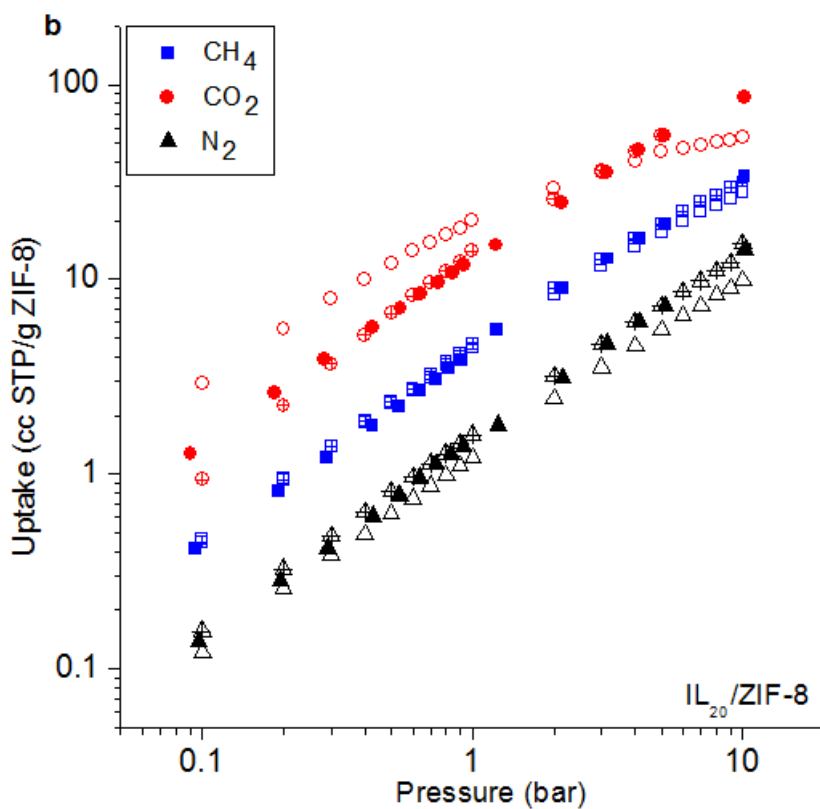
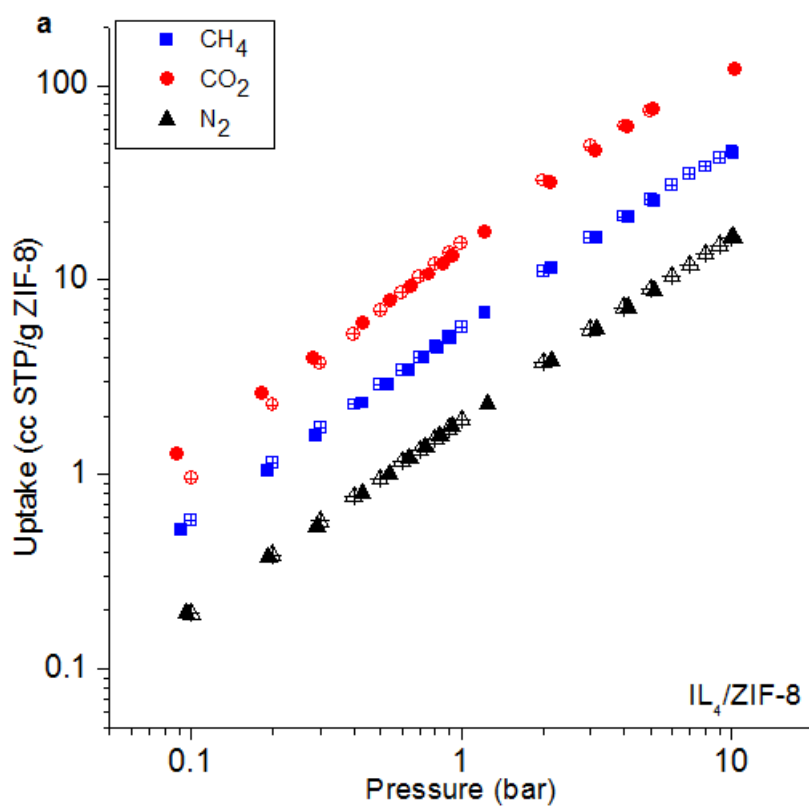


Figure C.2: Deconvoluted IR peaks between 2800-3200 cm^{-1} : (a) $\text{IL}_4/\text{ZIF-8}$, (b) $\text{IL}_{20}/\text{ZIF-8}$, (c) $\text{IL}_{28}/\text{ZIF-8}$, (d) ZIF-8 .

APPENDIX D: Gas Uptakes and Selectivities



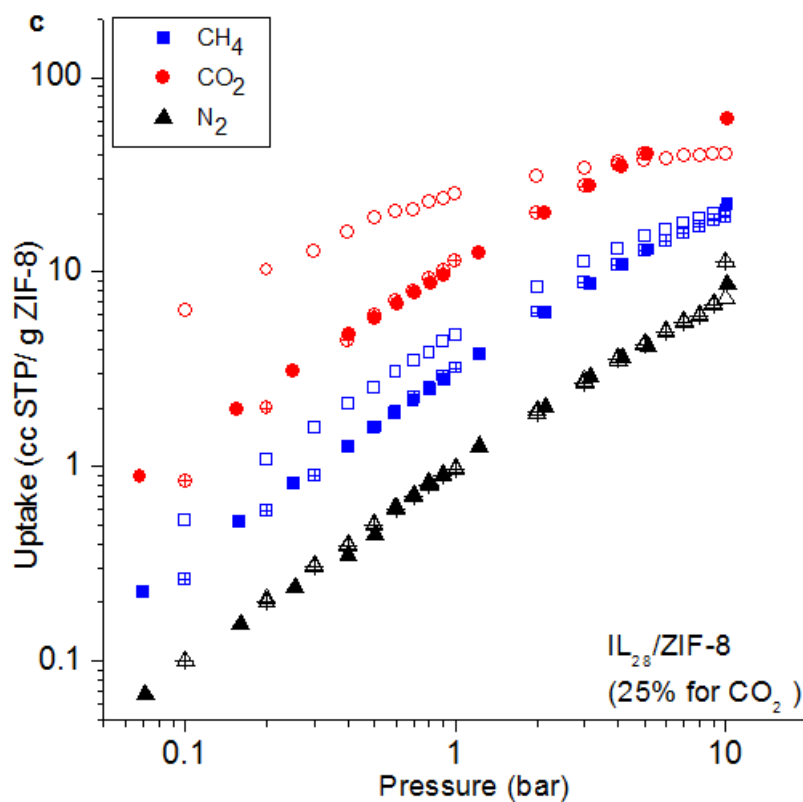
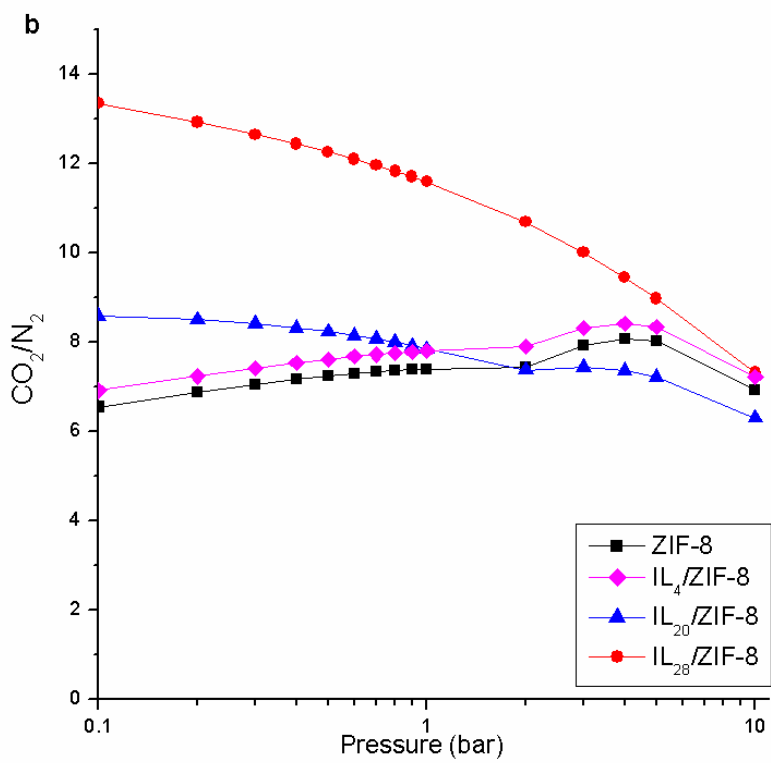
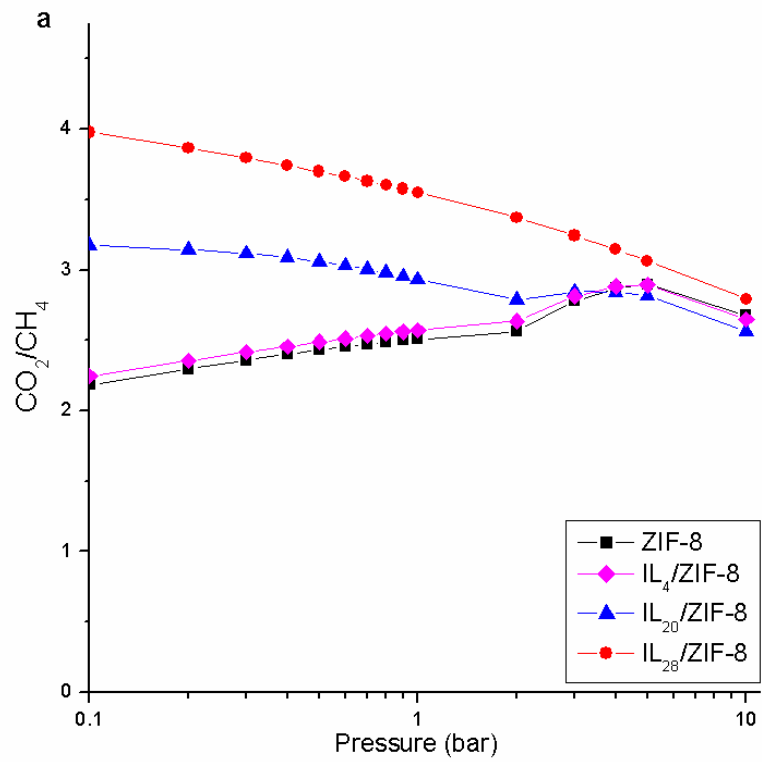


Figure D.1: Gas uptakes of ZIF and IL-incorporated ZIF-8 obtained from experiments and simulations (a) IL₄/ZIF-8, (b) IL₂₀/ZIF-8, (c) IL₂₈/ZIF-8. Filled symbols: experimental uptake values, empty symbols: unmodified computational uptake values, plus circle: computational uptake values scaled with the factor.



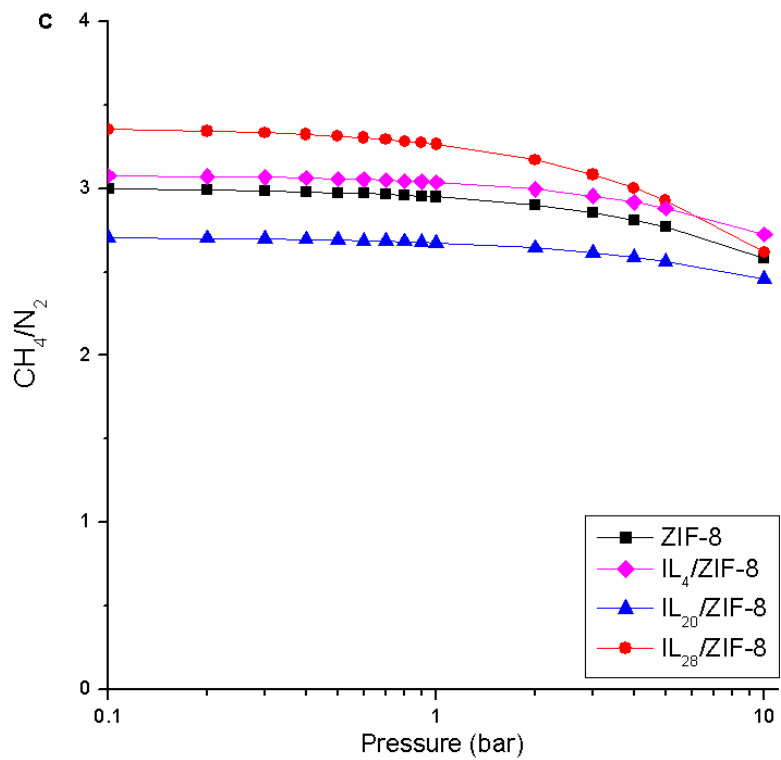


Figure D.2: Ideal adsorption selectivities of ZIF-8 and [BMIM][BF₄]/ZIF-8 samples calculated from fitted isotherms.

APPENDIX E: Names of Ionic Liquids

Table E.1: Full names of ionic liquids mentioned in this thesis.

IL Abbreviations	Full Name
[BMIM][Cl]	1-Butyl-3-methylimidazolium chloride
[BMIM][Br]	1-Butyl-3-methylimidazolium bromide
[BMIM][Cys]	1-Butyl-3-methylimidazolium 2-amino-3- mercaptopropionic acid (L-cysteine)
TEDA-BAIL	Triethylene diamine based Brønsted acidic imidazole based ionic liquid
ABIL-OH	amino-functionalized basic IL
[PSMIM][HSO ₄]	1-Methylimidazolium-3-propylsulfonate hydrosulfate
DAIL	Dual amino-functionalized ionic liquid
[BMIM][PF ₆]	1-Butyl-3-methylimidazolium hexafluorophosphate
[BMIM][SCN]	1-Butyl-3-methylimidazolium thiocyanate
[EMIM][EtSO ₄]	1-Ethyl-3-methylimidazolium ethyl sulfate
[BMIM][BF ₄]	1-Butyl-3-methylimidazolium tetrafluoroborate
[BMIM][Tf ₂ N]	1-Butyl-3-methylimidazolium bis(trifluoromethylsulfonyl)imide
[EMIM][Ac]	1-Ethyl-3-methylimidazolium acetate
[vbim][NTf ₂]	1-Vinyl-3-butylimidazolium-bis(trifluoromethyl- sulfonyl)imidate
[emim][B(CN) ₄]	1-Ethyl-3-methylimidazoliumtetracyanoborate
[(EtO) ₂ IM][NTf ₂]/ZIF-8	1,3-Diethoxyimidazolium bis(trifluoromethylsulfonyl)imide
[EMIM][PF ₆]	1-Ethyl-3-methylimidazolium hexafluorophosphate
[OMIM][PF ₆]	1-Methyl-3-octylimidazolium hexafluorophosphate
[C ₃ CNMIM][NTf ₂]	1-(3-Cyanopropyl)-3-methylimidazolium bis(trifluoromethylsulfonyl)amide
[EMIM][SCN]	1-Ethyl-3-methyl-imidazolium-thiocyanate
[BMIM][OcSO ₄]	1-Butyl-3-methylimidazolium octylsulfate